



SINTEF Energy Research
NO-7465 Trondheim
NORWAY



Energétique et Environnemen
69 621 Villeurbanne
FRANCE

5th year Internship
Presented by HAMRAZ Amir

PARTICLE DEPOSITION ON CYLINDER IN A CROSS FLOW

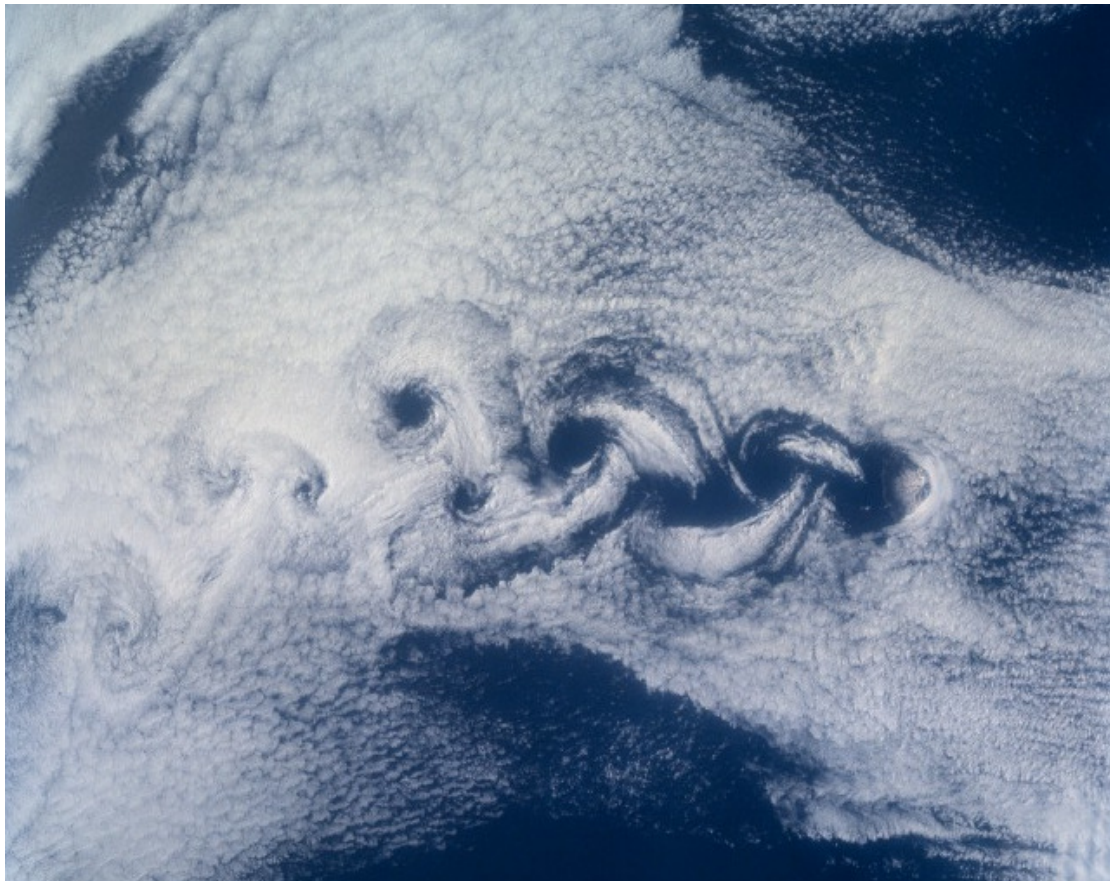


(Image form NASA)
April the 1st to August 15th

Supervisor: Nils Erland L. HAUGEN
Professor: Ronnie KNIKKER

Acknowledgements

I would like to give special thanks to Dr. Nils Erland HAUGEN, for the chance he gave me to carry out my internship on this project at SINTEF Energy Research, as well as for his time and help. I would also like to thank Professor Ronnie Knikker for his advice.

I also want to thank Dr. Steinar Kragset, the combustion crew as well as the main-office crew for their support.

Abstract

Particle depositions on the surface of heat exchanger decrease their performance. Finding the way to reduce the deposition of particles has a great interest. This phenomenon depends strongly on particle size and the Reynolds number of the flow. The purpose of this study is to investigate the deposition of particles in 3-D using direct numerical simulation (DNS). The current internship has contributed to develop the numerical code used to run the simulations. A review of the different works published on the topic has been done in order to provide a comparative basis. The problem is modeled as a circular cylinder in a cross flow, with a constant mass flow at the inlet boundary. This device allows us to simplify the problem while watching the phenomena surrounding the fundamentals mechanisms. The study is particularly focused on the Strouhal number as a function of Reynolds number. The Strouhal number as we will see in our study allows to characterize the Van Karman street occurring downstream of the cylinder. These paths play a very important role in the deposition of particles on the surface of our cylinder.

La déposition de particule sur les surfaces des échangeurs est l'une des principales causes de diminution de leur rendement. Découvrir une manière de baisser les dépôts de particules est un enjeu majeur dans plusieurs domaines tels que le chauffage ou la climatisation. Le phénomène dépend fortement de la taille des particules et du nombre de Reynolds. Le but de cette étude est d'étudier la déposition de particules en 3-D en utilisant le DNS (simulation numérique directe). Le présent stage a contribué à développer le logiciel qui utilisé pour les simulations numériques. Le problème est modélisé comme un cylindre placé dans un tuyau avec un débit constant à l'entrée. Ce dispositif nous permet de simplifier le problème tout en regardant les phénomènes fondamentaux qui entourent ce mécanisme. Ici, on s'intéresse tout particulièrement à la variation du nombre de Strouhal en fonctions du nombre de Reynolds. Ce nombre, Strouhal, comme on verra dans notre étude permet de caractériser les allées de Van Karman qui se produisent en aval d'un cylindre à section circulaire ou à section carrée. Ces allées jouent un rôle capital dans la déposition de particules sur la surface de notre cylindre.

Contents

<i>Acknowledgements</i>	2
<i>Abstract</i>	3
<i>Nomenclature</i>	5
<i>Introduction</i>	7
A- FLUID DYNAMICS THEORY	9
I- The fundamental equations	9
II- Conceptual overview of flow	11
III- Vortex shedding	17
IV- Three dimensional vortex dynamics in wake transition	19
B- THE SIMULATION CODE DESCRIPTION	27
I- DNS review	27
II- Pencil-code presentation	28
C- RESULTS AND ANALYSIS	30
I- Simulation approach	30
II- Results	36
III- Critical view	41
<i>Conclusions</i>	42
<i>Appendix</i>	43
Appendix A: Hopf bifurcation	43
<i>Bibliography</i>	45

Nomenclature

x, y, z : Axial component (m)

t : Time (s)

μ : Dynamic viscosity ($kg.m^{-1}.s^{-1}$)

ρ : Density of the fluid ($kg.m^{-3}$)

ν : Kinematic viscosity, equal to $\frac{\mu}{\rho}$ ($m^2.s^{-1}$)

Re : Reynolds number

P : Atmospheric Pressure during test (Pa)

T : Fluid temperature (K)

S : Strouhal number

f : Frequency of the vortex shedding (s^{-1})

u : Fluid velocity ($m.s^{-1}$)

u_0 : Inlet fluid velocity ($m.s^{-1}$)

L : Characteristic length (m)

∇ : Divergence

τ_{ij} : Stress tensor

S_{ij} : Rate of strain tensor (s^{-1})

F_{p-f} : Particles force acting on the fluid (N)

$()^T$: Transpose of a matrix

x : Particle position

V : Particle velocity ($m.s^{-1}$)

m_p : Particle mass

F_p : Particle forces (N)

τ_f : Fluid time scale

τ_p : Particle time scale

θ : Oblique angle of eddies ($^{\circ}$)
 θ_s : Separation angle ($^{\circ}$)
 $-C_{Pb}$: Base suction coefficient
 C_D : Drag coefficient
 q : Spanwise wave number
 dy : Cell size in y direction (m)
 λ : Wavelength, equal to $\frac{u}{f}$ (m)
 V : Particles velocity ($m.s^{-1}$)
 D : Cylinder diameter (m)
 L_W : Length of the recirculation zone (m)
 St : Stockes number
 Δt : Time step (s)
 Δx : Length interval (m)
 $C = CFL$: Courant–Friedrichs–Lewy condition
 L_{xyz} : Last corner of box
 xyz_0 : First corner of box
Tr W: Wake transition
Tr SL: Shear layer transition
Tr BL: Boundary layer transition
Tr: Turbulent transition
DNS: Direct numerical simulation
G-L: Ginzburg-Landau (G-L) equation

Introduction

The present internship has been carried out at SINTEF, within the department of Energy Research. This subdivision works in many areas of research. One of them is combustion and heat transfer, which is the laboratory where the work described in this report, was carried out.

In boilers where either bio-mass or municipal solid waste is used as the primary fuel there are huge problems related to particle deposition on the boiler tubes, in particular in the super-heater. The deposited particles create an insulating layer on the tubes, preventing the hot exhaust gas from heating the water/steam inside the tubes and thus reducing the efficiency of the plant. Current CFD simulations neglect the effect of turbulence on the particle deposition even though it is believed that for not too large turbulent intensities the deposition of sub-micron particles is partly controlled by the turbulence. The aim of this project is to develop and verify the numerical code which will be used for this study: namely the Pencil-Code (Nordita). This is an open source direct numerical simulation (DNS) code. It uses a high order finite-difference scheme for compressible hydrodynamic flows. The current report describes a review of previous investigations together with the present results. A study carrying out particle deposition in 2 dimensions was done last year (2008) in order to find if deposits will form and how the deposits depend on Reynolds and Stokes Numbers.

Particle-loaded flows around bluff bodies are also frequently encountered in nature and industrial applications, such as the aerosol flow past building or as mentioned above combustion gas containing dispersed particles flowing round tubes of a heat exchanger. The flow around circular cylinder can be taken as a representative case for the flow around a bluff body. It is quite complex problem because the flow will not follow the circular cylinder completely, but separates from it and creates wakes. As a result, there are three components in this flow: a boundary layer, a separating free shear layer and a wake. The generation and shedding of large coherent vortex structures due to flow, make the flow around the circular cylinder very difficult to predict. For more than a century, a lot of studies have focused on it.

In 1912 Von-Karman found the stability of vortex street configuration and also a theoretical link between the vortex street and the drag on the body. In 1954 Roshko was the first to observe the existence of the different regimes and the transition regime. In 1992 Williamson discovered the appearance of vortex dislocation and observed two different modes of formation of streamwise vortices. To characterize these transition regimes, many parameters have been used like: Strouhal number, the separation point, the recirculation length and coefficients of lift and drag (Zdravkovich, 1997; Williamson, 1996a; Williamson, 1992; Williamson, 1989)

Many studies on the particle deposition have been done very recently (Burger, 2006; Luo, et al., 2008) due to the many new different characteristics related to the circular cylinders and mostly the recent numerical and simulation capacity.

Particle deposition is determined by the inertia of the particle and by the motion of the fluid. The Stokes number is a dimensionless measure of the ratio between a particles dependence on its own inertia and its dependence on the motions of fluid. There are many different deposition mechanisms but as shown in a previous report (*Project no: 019809*) the impaction is normally the most important mechanism in particles deposition. It is 50 to 100 times faster than the other ones.

In order to simplify the study, we have focused on a simple geometry. In two dimensions, we assume a cylinder in a cross flow, where the flow is between two infinite parallel plates and is not in contact with any of the plates. The distances between the plates and their length are variables; you can see these results in section C. In three dimensional simulations, we assume that the cylinder is in a cube, this cube has the same dimensions in x and y direction as in 2-D simulation but the cylinder has a finite extent in the z direction.

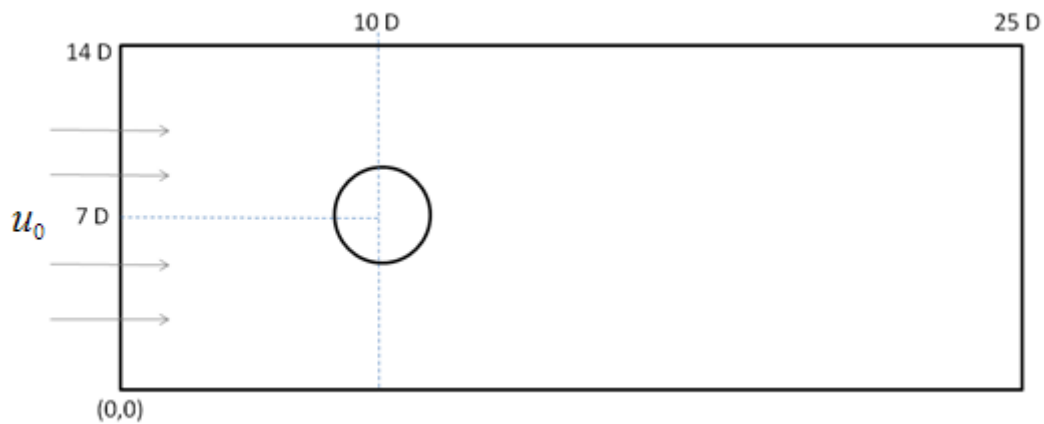


Figure 1: 2-D Sketch of the computational domain

A- FLUID DYNAMICS THEORY

Even though the purpose of the present work is not to define the vortex street in detail, it is important to give a general vortex definition in cylinder wake in order to understand the physics. Therefore, the goal of this section is to describe the different equation used and to provide elements allowing to understand the different behavior in three dimensional wake transition. This section is inspired by the work of Williamson, 1996a; Williamson, 1996b and Zdravkovich, 1997.

I- The fundamental equations

The fluid equations are written in an Eulerian formalism, while the particle transport equations are written in Lagrangian formalism.

1- The fluid equations

The equations to be solved for the fluid are essentially the Navier-Stokes equations which consist of the continuity equation:

$$\frac{\partial \rho}{\partial t} + \nabla \cdot (\rho \mathbf{u}) = 0 \quad (1)$$

and the momentum equation

$$\frac{\partial \mathbf{u}}{\partial t} + \mathbf{u} \cdot \nabla \mathbf{u} = -\frac{1}{\rho} \nabla P + \nabla \cdot \boldsymbol{\tau} + \frac{\mathbf{F}_{p-f}}{\rho} \quad (2)$$

Where ρ is the fluid density, \mathbf{u} is the velocity vector, P is the pressure, $\boldsymbol{\tau}_{ij} = 2\rho\nu\mathbf{S}_{ij}$ is the stress tensor, $\mathbf{S}_{ij} = \frac{1}{2} (\nabla \mathbf{u} + (\nabla \mathbf{u})^T) - \frac{1}{3} \nabla \cdot \mathbf{u}$ is the traceless rate of strain tensor, ν is the kinematic viscosity, \mathbf{F}_{p-f} is the force acting from the particle on the fluid. For DNS the above equations are indeed the equations which are solved.

2- The particles equations

The equations for particles position, velocity and rotation are solved in the Lagrangian formalism. This means that we follow each particle while it moves through the domain. The equation for particle position, \mathbf{x} , is:

$$\frac{d\mathbf{x}}{dt} = \mathbf{v} \quad (3)$$

And the equation for the particle velocity, \mathbf{v} , is:

$$\frac{d\mathbf{v}}{dt} = \frac{1}{m_p} \sum \mathbf{F}_p \quad (4)$$

Where
$$\sum \mathbf{F}_p = \mathbf{F}_D + \mathbf{F}_g + \mathbf{F}_L + \mathbf{F}_{p-p} + \mathbf{F}_T + \mathbf{F}_B + \mathbf{F}_w \quad (5)$$

F_p is the addition of: F_D is the drag force, F_g is the gravity force, F_L is the lift force, F_{p-p} is the inter particle force, F_T is the thermophoretic force, F_B is the force due to Brownian motions and F_w the particle wall force.

3- Non dimensional numbers

a) The Reynolds number

The Reynolds number Re is a dimensionless number that gives a measure of the ratio of inertial forces ($U \cdot \rho$) to viscous forces (μ / L) and, consequently, it quantifies the relative importance of these two types of forces for given flow conditions. The Reynolds number is defined as:

$$Re = \frac{\rho \cdot U \cdot L}{\mu} \quad (6)$$

It is also used to characterize different flow regimes, such as laminar or turbulent flow.

b) The Strouhal number

The Strouhal number is a dimensionless number describing oscillating flow mechanisms. The Strouhal number represents a measure of the ratio of inertial forces due to the unsteadiness of the flow or local acceleration to the inertial forces due to changes in velocity from one point to another in the flow field. The Strouhal number S is defined as:

$$S = \frac{f \cdot U}{L} \quad (7)$$

When f is the frequency of vortex shedding, L is the characteristic length (for example hydraulic diameter) and U is the velocity of the fluid.

For large Strouhal numbers (order of unity), viscosity dominates the flow, resulting in a collective oscillating movement of the fluid "plug". For low Strouhal numbers (order of 10^{-4} and below), the high-speed, quasi steady state portion of the movement dominates the oscillation. Oscillation at intermediate Strouhal numbers is characterized by the build up and rapidly subsequent shedding of vortices. (Sobey, 1982).

c) The Stokes number

The Stokes number is a dimensionless number corresponding to the behaviour of particles suspended in a fluid flow. The Stokes number is defined as the ratio of the stopping distance of a particle to a characteristic dimension of the obstacle. It is a measure of the ratio between a particles dependence on its own inertia, particle time scale τ_p and its dependence on the motions of the fluid which is represented by time scale of fluid τ_f , i.e.:

$$St = \frac{\tau_p}{\tau_f} \quad (8)$$

For $St \gg 1$, particles will continue in a straight line as the fluid turns around the obstacle therefore impacting on the obstacle. For $St \ll 1$, particles will follow the fluid streamlines closely.

II- Conceptual overview of flow

1- Definition

When a fluid flows past a stationary body a region of disturbed flow is always formed around the body. The extent of the disturbed flow region is largely dependent on the shape, orientation and Reynolds number. The flows around all bluff bodies have some similarities and circular cylinders put together many of these similarities. The disturbed flow region is characterized by the variation of a local velocity in magnitude, direction and time. The velocity average may be greater than, equal to, or less than the free stream velocity in different area around the cylinder. Figure 2 shows the division of the flow into four regions:

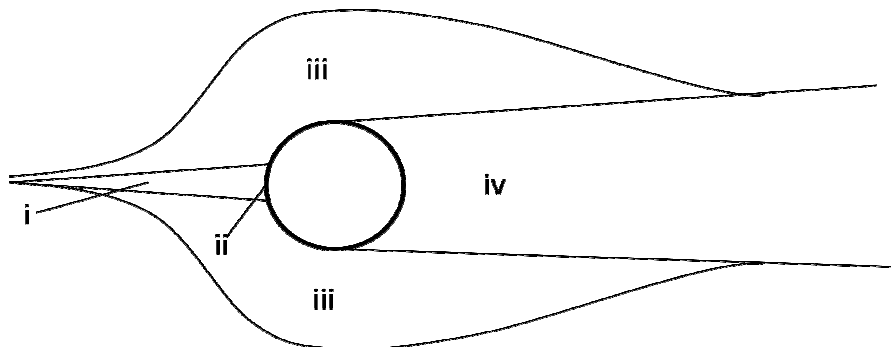


Figure 2*: Regions of distributed flow

- i) One narrow region of retarded flow or stagnation region
- ii) Boundary layers attached to the surface
- iii) Two sidewise regions with accelerated flow
- iv) One wide downstream region of separated flow called the wake.

Most past research has been focused on the wake region. Large flow structures are formed in the near wake and gradually decay along the wake. A particular feature of

the flow is a succession of transitions in various regions of distributed flow (Roshko, et al., 1969). Figure 3 shows the development of transitions with Re in three distributed region: Wake (TrW), shear layer (TrSL) and boundary layers (TrBL):

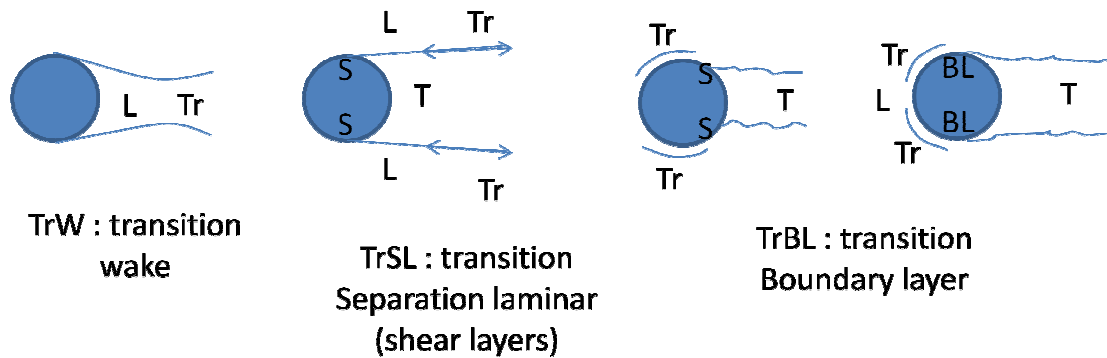


Figure 3*: Different wake behind cylinder

There are five principal regimes: Laminar, Transition in wake state of flow, Transition in shear layers, Transition in boundary layer and at the end fully turbulent state of flow. Each regime can be subdivided to different sub-regimes. We try to have an overview on the various flow regimes. As our basis we will use the plot of base suction coefficient ($-C_{pb}$) (Williamson, 1996b) and drag coefficients (Zdravkovich, 1997).

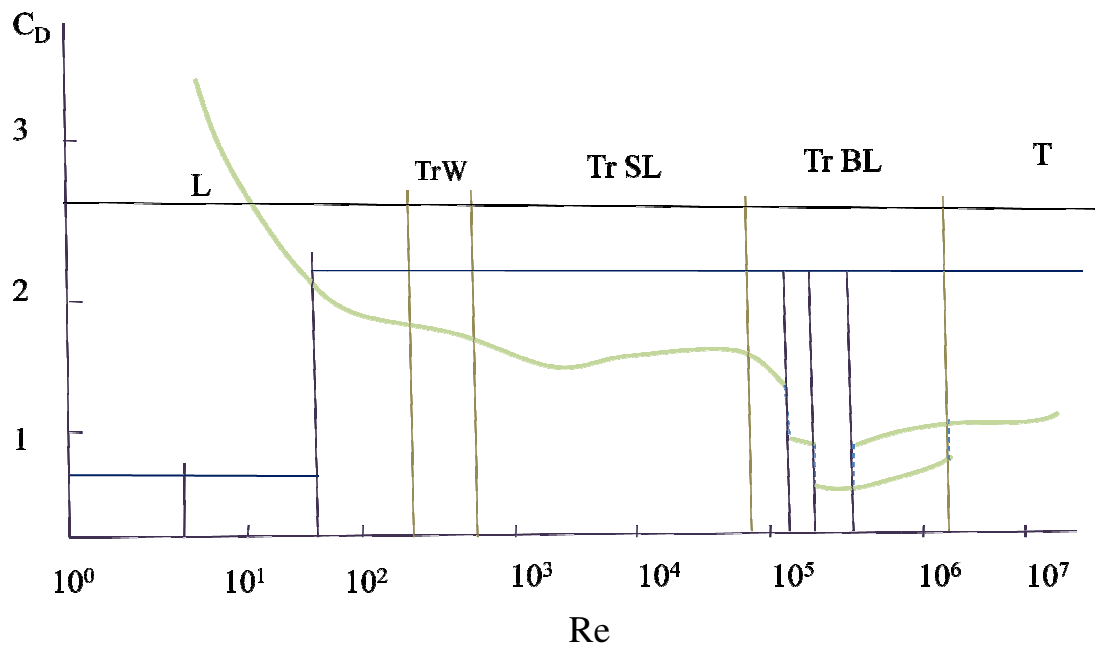


Figure 4*: Drag coefficients as a function of Reynolds number, different regimes are indicated

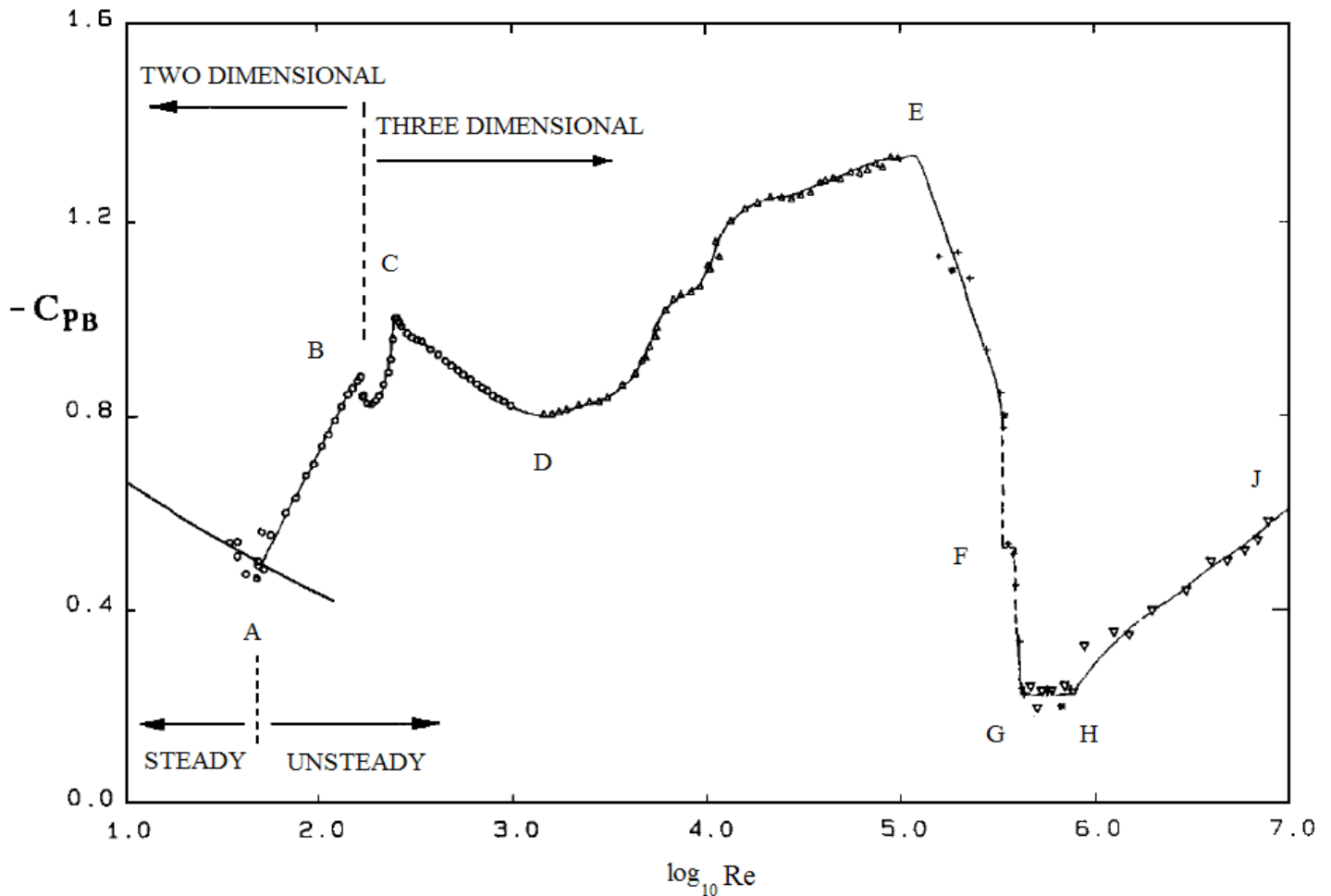


Figure 5*: Plot of base suction coefficient ($-C_{PB}$). The base suction coefficient is a measure of the vacuum level behind the cylinder

The range of Re in which our works take place goes up to 700. And a particular attention would be given to wake transition regime ($Re \sim 190$ to 260).

2- Governing and influencing parameters

The Reynolds number has been singled out as the governing parameter for idealized free stream flows. But the real flows around cylinders in many applications are affected by a wide variety in parameters, qualified as influencing parameters. Sometime an influencing parameter can become a governing parameter when its importance exceeds some value. Some typical examples of the most frequently encountered influencing parameters are irregular, steady and periodic disturbances. Free stream turbulence, described with turbulence intensity is one of the most common disturbances. Surfaces roughness, wall blockage, wall proximity, end effects, free end, transverse oscillation and streamwise oscillations are the others influencing parameter (Zdravkovich, 1997).

3- Different flow regimes

- Laminar steady regime Re 5-47

At Re below around 47, the wake comprises a steady recirculation region (L_w) of two symmetrically placed vortices on each side of the wake. The length of the wake grows as the Reynolds number increases. (See section D) There is a linear empirical relationship for this regime when there is no wall blockage:

$$\frac{L_w}{D} = 0.05Re, \quad 4.4 < Re < 47 \quad (9)$$

- Laminar vortex shedding Re 47-190

The steady and closed near wake becomes unstable and the transversal oscillation starts at the end of near wake. Their strength and instability grow with Re and the formation length decrease. The onset of the wake instability is near $Re=47$ and it is a manifestation of Hopf bifurcation (Wikipedia) (*Appendix A*). The wake oscillations are purely periodic over this regime and that is why sometime this regime is also named the periodic laminar regime. The vortex shedding is normally parallel to the cylinder. See Figure 6.

- Wake Transition Regime Re 190-270 3-D

This transition regime (2-D toward 3-D) is associated with two discontinuous changes in the wake formation as Re is increased (see Figure 6). The wake transition state of the flow is associated with transition to turbulence in the wake. This means that all eddies are formed laminar and become turbulent downstream. At $Re=190$ we can see the deformation of the vortices as they shed, at wavelength around 3-4 cylinder diameters, that is creating the first discontinuity. This first discontinuity is named “hard transition” in opposition with the second one and it is also hysteretic. In the second discontinuous change in the St-Re relation, there is a gradual transfer of energy from mode A shedding to a mode B shedding over the range 230-250. The latter mode comprises finer-scale streamwise vortices, with a spanwise length scale of around one diameter.

In this regime we can see large intermittent low frequency irregularities, which are caused by a phenomenon named vortex dislocation. These low frequencies indicate the instabilities of the velocity fluctuations in the wake. The separation angle, θ_s , can be estimated in the range $95^\circ < \theta_s < 115^\circ$. Note that the higher values of θ_s correspond to lower Re and vice versa.

This regime will be discussed in depth in the next paragraph.

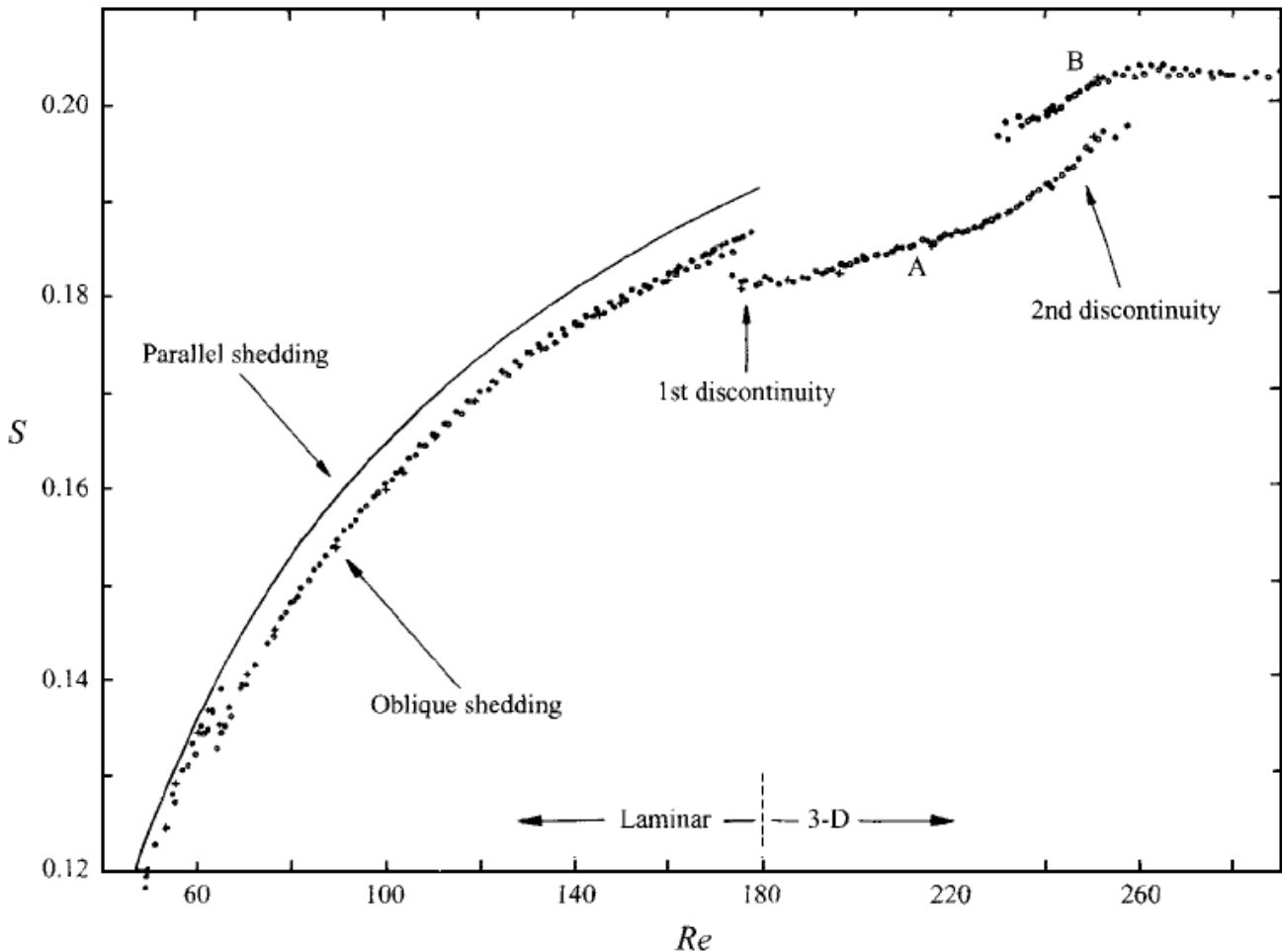


Figure 6*: Strouhal-Reynolds number relationship over laminar and three-dimensional transition regimes. (Taken from Williamson (1988, 1992))

- Lower subcritical flow regime Re 270 – 1000

This regime starts with the peak in base suction, see point C in Figure 5, which is associated with the ordered 3-D streamwise vortex structure in the near wake. The fine scale streamwise vortex structure becomes highly disordered and the strength of the turbulent eddies decreases rapidly downstream. As Re increase, the drag coefficient decreases and the eddy formation region elongates.

- Shear-Layer Transition Regime $Re=1000$ to 200000

In the shear layer transition regime the base suction increase, Strouhal number gradually decrease (for Re over 110000) and the formation length decreases to. These are caused by the developing instability of the separating shear layers from the sides of the body. Bloor (Bloor, 1964) found that the instability vortices appearing in the shear layer generate frequencies in the wake that varied as $Re^{3/2}$, rather than as Re for the Karman vortices. In this regime there is the 2-D Kelvin-Helmholtz instabilities which create the base suction rising.

In shear layer transition regime, the eddy shedding takes place in High-speed mode. Eddies are formed behind the cylinder by the wrap of free shear layers in an approximately fixed position. The eddy street starts by the alternate shedding of fully grown eddy. Gerrard (Gerrard, 1966) says than high speed eddy shedding mode depends on four parameters:

- i) The distance between the free shear layers (width of near-wake)
- ii) The force of the eddy
- iii) The thickness of boundary layer
- iv) The boarding into near-wake

- Critical regime

This regime corresponds to the discontinuity occurred on the drag force. As you can see in Figure 2, for the regime Tr BL, there are two discontinuities on the curve. There are related to the separation bubble in the each side of the cylinder.

The first discontinuity is caused by a laminar separation bubble forming on one side of the cylinder (up or down). This separation does not affect the free shear layer development in other side. By increasing Re the shear layer separated in other side too and the second discontinuity appears. Remark than this regime has a narrow range of Re in comparison with other flows. To be more precise they are not really the discontinuities but the transition is so fast between the different regimes than, it could be considerate like a discontinuities.

- Supercritical regime

As said previously the critical regime became symmetric and there are the separated bubbles in each side of the cylinder. Increasing Re , Strouhal number grows up (around 0.4) and the eddy shedding is disrupted and the transition starts to occur in the boundary layer and it is very irregular.

- Post-critical Regime

The effect on an increase in Re is to move the turbulent transition point before the cylinder that meant the boundary layer in surface is turbulent. The most surprising result demonstrated by Roshko in 1961 (Roshko, 1961), is that, there is a periodic vortex shedding in the flow behind the cylinder.

For more information about the Lower subcritical flow regime, Shear-Layer Transition Regime, Critical régime, Supercritical regime, Post-critical Regime you could refer to M.Zdravkovich book flow around circular cylinder Volume 1 (Zdravkovich, 1997).

III- Vortex shedding

Depending on the flow regimes, different modes of vortex shedding are available. In the current project, the S-Re curve has been chosen. On other hand, it happens that the real vortex shedding and those simulated with DNS or other simulation codes vary.

1- Laminar case

There are two different modes of vortex shedding: oblique and parallel. For years there has been an extensive research in order to understand and determine which one is the most appropriate for the vortex shedding. However, today one knows that the different shedding modes and discontinuities in between Strouhal number and Reynolds number in laminar regimes are directly related. In the hypothesis of ideal conditions, i.e. no shears in free stream or cylinder vibration, the discontinuities in S-Re relation around $Re = 65$ are due to the oblique shedding. See Figure 6.

The oblique shedding depends strongly on the boundary conditions at the spanwise tips of the cylinder. These boundary conditions dictate the shedding angle over the whole span. The near regions to the tips (until around 10 diameters in length) are directly influenced and have lower frequencies. The influence of the different frequencies along the span can be seen even for very long cylinders (until around $2000D$ long). The typical oblique shedding angles are around $15-20^\circ$. These different frequencies create the vibrations that cause discontinuities in S-Re relation.

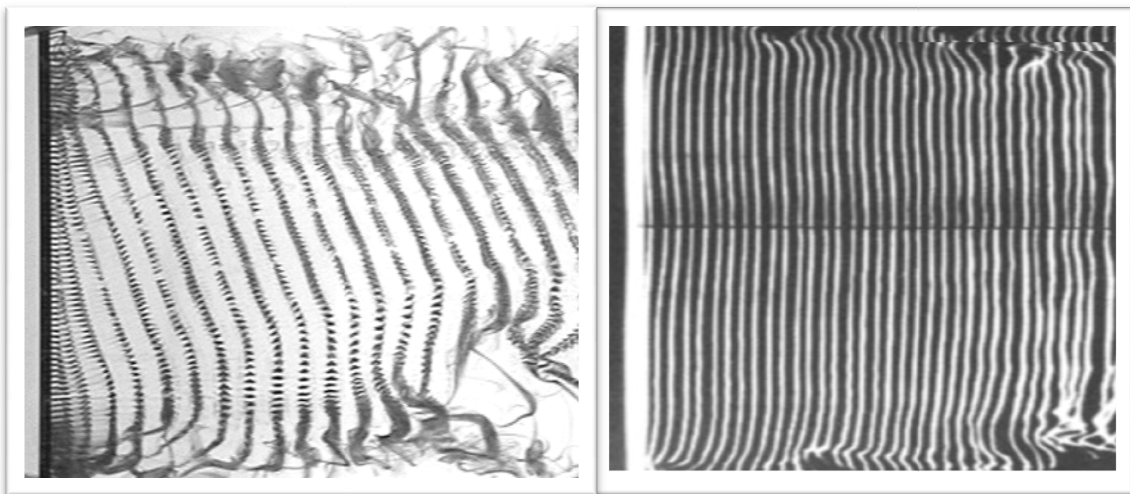


Figure 7*: Example of oblique (left) and parallel (right) shedding for $Re=140$

There are various techniques in order to achieve parallel shedding: angled endplates (Williamson, 1989), coaxial cylinders at the tips of the main cylinder (Eisenlohr, et al., 1989) or suction tubes from downstream (Miller, et al., 1994). As shown in Figure 6, with parallel shedding the S-Re curve is completely continuous. Williamson has then shown that parallel shedding is the universal one. Oblique shedding can be collapsed onto a parallel shedding curve by using the below transformation:

$$S_{Parallel} = S_{oblique} \cdot \cos \theta \quad (10)$$

When θ is angle of oblique wave and S is Strouhal number (Williamson, 1988).

2- Three dimensional shedding mode

3-D vortex shedding involves many different components like parallel and oblique shedding, cellular shedding, vortex dislocations, phase shocks and phase expansions and the high speed parameters defined by Gerrard (Gerrard, 1966) (*see Shear-Layer Transition Regime*).

The vortex dislocations are specific to three dimensional wake transitions, and are further discussed in the next section.

The shock and expansion phases are predicted by a particular form of Ginzburg-Landau (G-L) equation, Burgers equation. (Monkewitz, et al., 1993)

$$\frac{\partial q}{\partial t} = \mu \frac{\partial^2 q}{\partial z^2} - \lambda q \frac{\partial q}{\partial z} \quad (11)$$

When q is the spanwise wave number, λ is wavelength and μ is dynamics viscosity. The solutions of this equation are shocks and expansion phases. In physical terms, these different phases depend on the different angles that are produced in cylinder wake. Miller & Williamson (Miller, et al., 1994) and Monkewitz (Monkewitz, et al., 1993) set up an experiment to show this phenomenon. They set up one angle across the complete span in the wake (oblique shedding) and they change impulsively the boundary conditions. If the angle generated downstream becomes greater than the initial angle, an expansion phase occurs. However, if the angle generated downstream is lower than the initial angle, a shock phase is produced.

With high Re numbers, the parallel and oblique shedding do not depend only on the ends conditions and the other factors remain without response.

3- Numerical simulation of vortex shedding

Today, DNS simulation remains the only approach to fully resolve the bluff body wake problem. Many parameters are very well predicted: drag and lift force, Strouhal number, and base pressure. The first point is associated with the onset of three dimensional wakes. Experimental devices show that the first discontinuity occurs at $Re = 190$ and shows hysteresis. However, in 3-D simulation this could be replaced by a continuous and smooth line, see Figure 6.

The difference between 2-D and 3-D simulations for the same Reynolds number is also studied. Mittal & Balachandar (Mittal, et al., 1995) and Karniadakis & Triantafyllou (Karniadakis, et al., 1992) have found that the difference between drag, lift or Strouhal number can be explained by the higher level of Reynolds stress** in 2-D case. This difference in Reynolds stress in the flow is associated with a shorter formation length as well.

Finally DNS enables us to see the vortex dislocations influence of Strouhal number in different regimes, especially in wake transition regimes. It has been shown that the Strouhal number is reduced by vortex dislocations, leading to the A mode in this regime, see Figure 13.

***In fluid dynamics, the Reynolds stress, R_{ij} , (or, the Reynolds stress tensor) is the stress tensor in a fluid due to the random turbulent fluctuations in fluid momentum. The stress is obtained from an average over these fluctuations.*

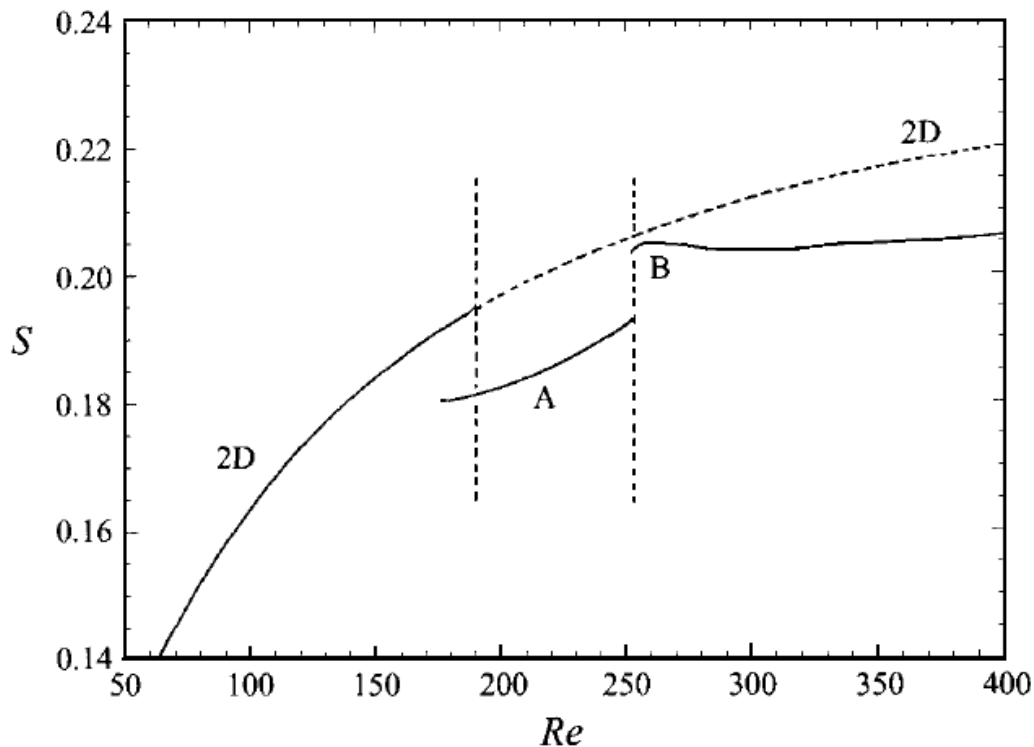


Figure 8*: Evaluation of Strouhal number value in 2-D and 3-D

IV- Three dimensional vortex dynamics in wake transition

The goal of this paragraph is to explain the evolution of this regime and the physical phenomenon associated with, and also how the vortex street can be generated. This regime is generally described by the Strouhal-Reynolds curve based on Williamson (Williamson, 1989) works, see Figure 6. It is not in the scope of this report to explain why these instabilities occur, since many questions are still not solved.

The transition from 2-D to 3-D vortex shedding occurs at Re around 190. At $Re = 190$, the first discontinuity occurs, the Strouhal frequency drops from the laminar curve to one corresponding to the mode A of 3-D shedding. This discontinuity shows hysteresis, which means that the exact Reynolds value for the transition depends on whether Re increases or decreases.

This mode is present up to $Re \sim 230-260$, there is a further discontinuity in Strouhal number, indicating transition to another mode of shedding, mode B. This mode is not hysteretic and involves a gradual transfer to energy from mode A to mode B. Each of these modes corresponds to different spanwise and streamwise instability in the wake.

1- Mode A shedding

It should be mentioned that the level of free stream turbulence and the end effects can influence the value of the critical Reynolds number in which the first discontinuity occurs. However, Barkley and Henderson (1995) have predicted by analytical studies that critical Re number is equal to 188.5 ± 1 . This value is in agreement with the experimental values.

Two different modes of 3-D shedding in this regime involve both spanwise and streamwise vorticity. The mode A shedding has an instability wavelength in the spanwise direction which is equal to four times the cylinder diameter ($4D$), while in B mode shedding the wavelength is more close to one cylinder diameter ($1D$). This is true for Reynolds numbers up to 10000, see Figure 9.

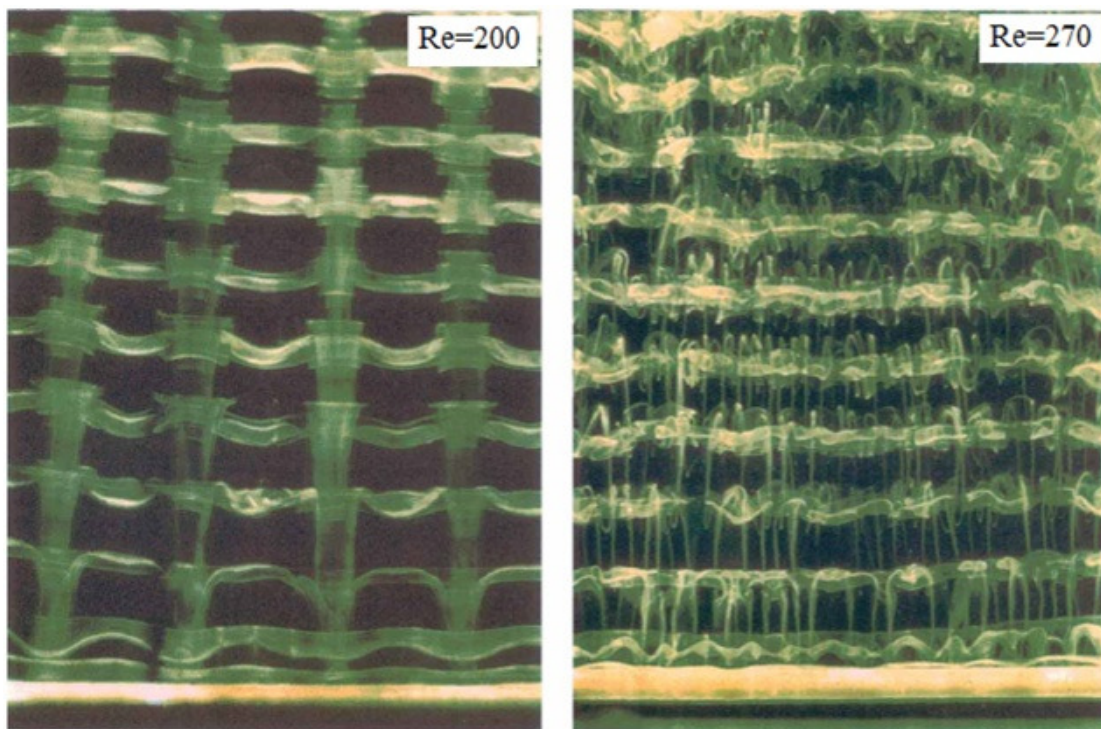


**Figure 9*: Modes A and B instabilities, mode A in left and B in right.
For Re=200 spanwise wavelength is $4D$ and $1D$ for Re=270**

The first shedding manner, mode A, is caused by an elliptical instability (Leweke, et al., July-August 1998) of the primary vortex. This instability produces the spanwise waviness and also the displacement of vortices toward the cylinder. The elliptical instability represents the exponential growth of inertial wave in the flow; it has been explained with a mathematical model, (Williamson, 1996b; Waleffe, 1990; Leweke, et al., July-August 1998). Here in Figure 10, we use a plot from Helene Persillon and Thomas Leweke, published by Williamson (Williamson, 1996b), to show a view of this elliptical instability. In Figure 10, the numbers show the values of strain rate. The regions in which the lines are aligned at 45° to the major axis of the ellipse show the 'elliptic' instability (red ellipse).

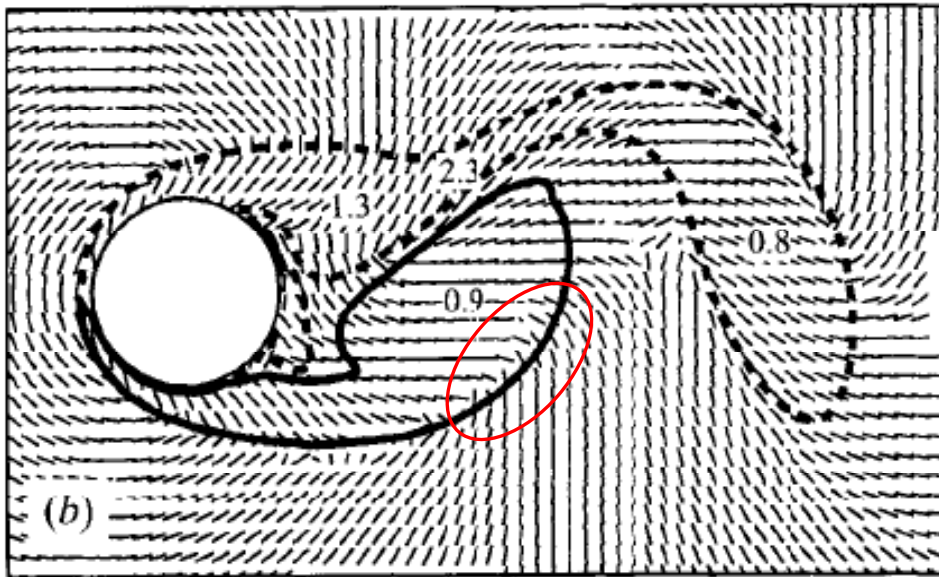


Figure 10*: Strain field from 2-D DNS at $Re=200$.

On other hand, the primary vortex is also pulled out by the cylinder. This mechanism continues from one primary vortex to the next, which means that in the spanwise direction the vortices become connected to each other, Figure 11. Influenced by the strain rate, the primary vortex becomes highly deformed. As we said the vortices in spanwise direction are connected, i.e. each vortex becomes deformed by the previous ones. In This manner all vortices in the spanwise direction are deformed. This attraction of the vortices toward the cylinder is caused by the reverse-flow region behind the body. These deformations occur at particular location along the cylinder. The distance between two locations is $4D$, Figure 9. The vortices in the streamwise direction come from this vortex deformation.

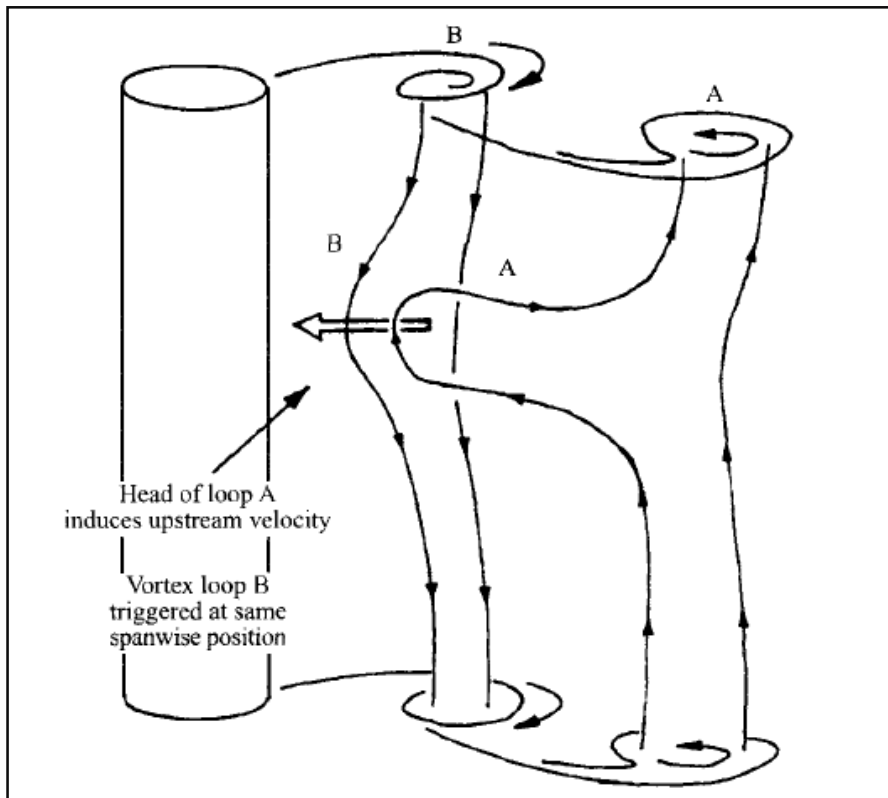


Figure 11*: Physical mechanism to produce vortex loop of mode A

Figure 12 shows how previous vortex point is attracted by the next vortex.

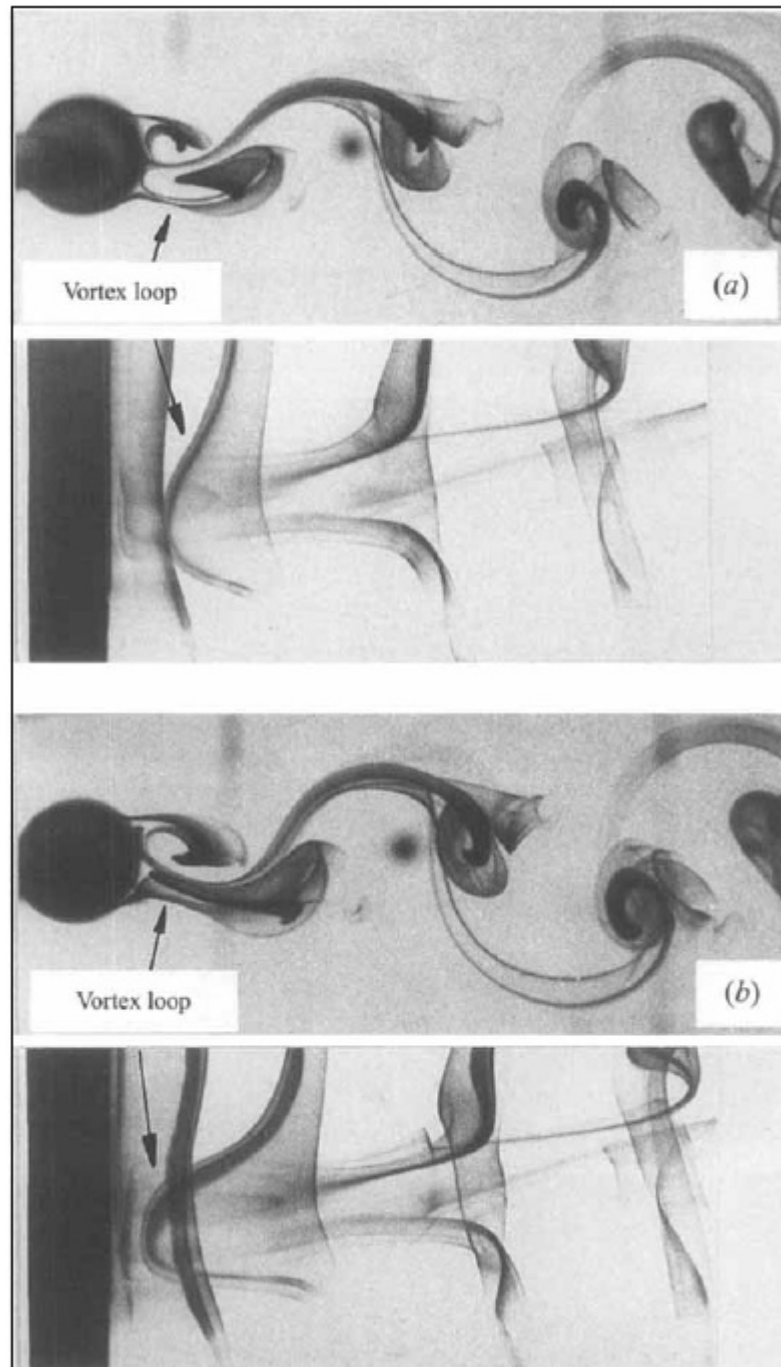


Figure 12*: Primary vortex pulled from the recirculation zone back upstream, while the rest of the primary vortex sheds into the wake

Also another phenomenon appears when 3-D mode shedding is generated. One can see low frequency irregularities in the vortex shedding process. It was discovered by Williamson (Williamson, 1992) that these irregularities are due to the existence of vortex dislocation in wake transition, see Figures 13 and 15. These vortex dislocations are generated between the spanwise vortices (cells). The vortex dislocation is a consequence of the growth of large vertical structures in the wake. This phenomenon is a fundamental feature of wake transition in mode A. As we can see in Figure 13 the vortex dislocations generate a drop in Strouhal number value. The difference between the purely small-scale instabilities (curves A and B) and these instabilities combined

with intermittent vortex dislocation (curves A* and B*) is shown in figure 13. The natural wake transition follows the sequence (2-D \rightarrow A* \rightarrow B).

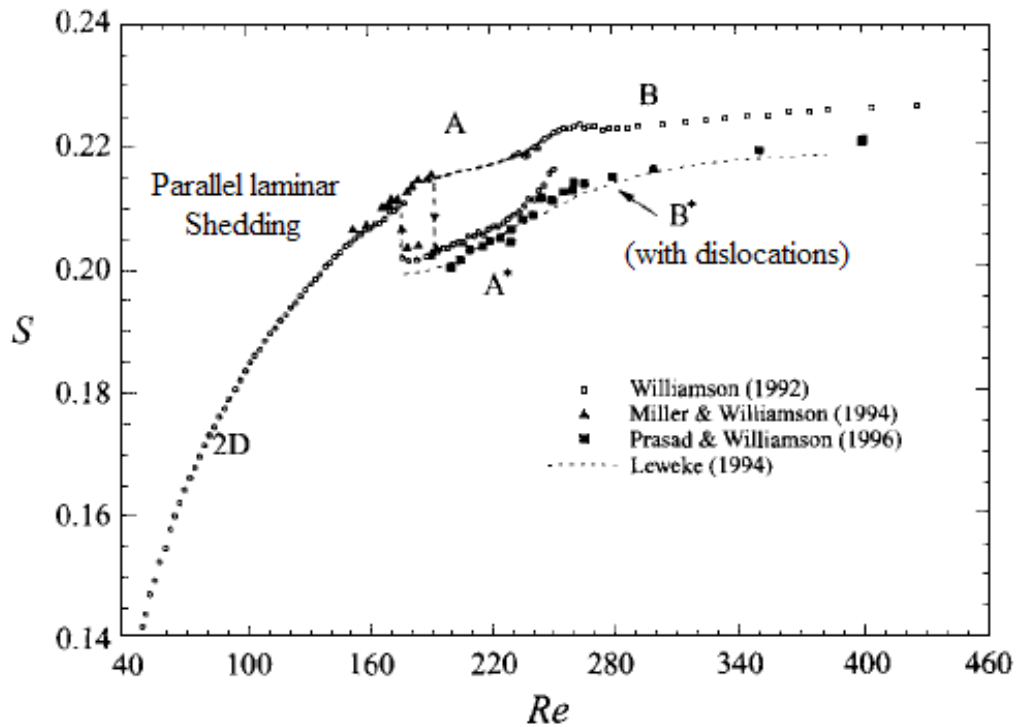


Figure 13*: Vortex dislocation effects on St-Re curve, the natural wake transition follows the sequence (2-D \rightarrow A* \rightarrow B)

On the other hand, the streamwise vortices in mode A are out-of-phase. This means that the streamwise vortices on two consecutive eddies have different signs, see Figure 14. Whereas, in mode B the streamwise vortices are called in-phase. We can see this phenomenon also in Figure 16.

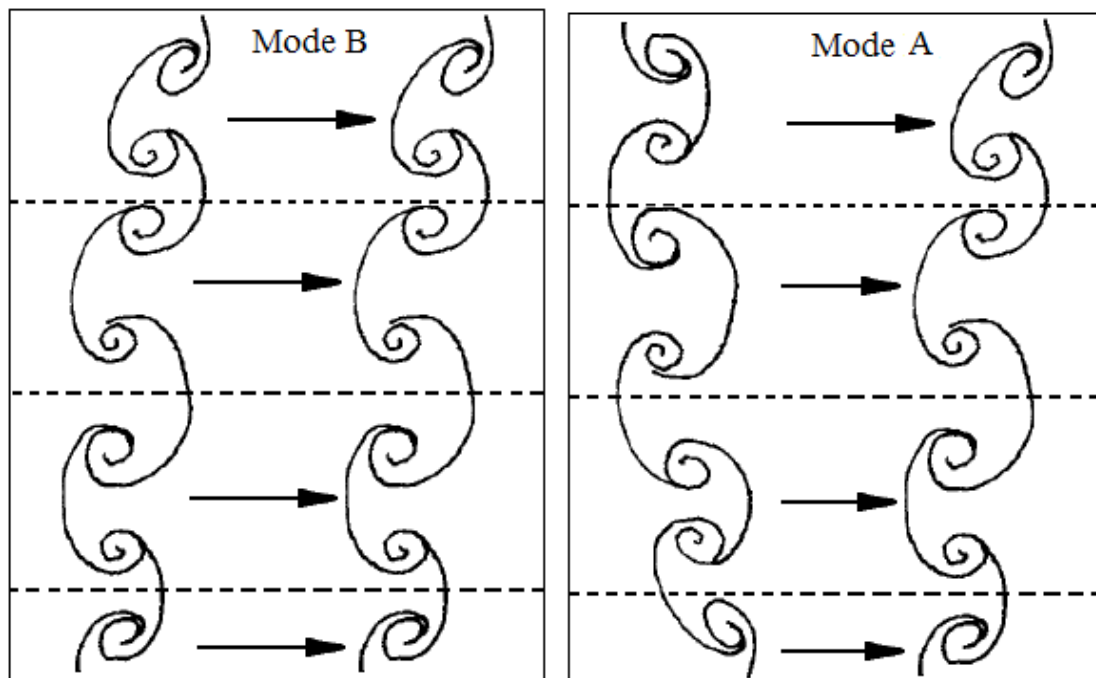


Figure 14*: In-phase streamwise vortex symmetry for mode B and out of phase for Mode A.

Later, DNS results showed that the gradual transfer of energy from mode A to mode B permit the presence of both modes after a certain value of Re . Modes A and B have the same energy close to $Re = 245$.

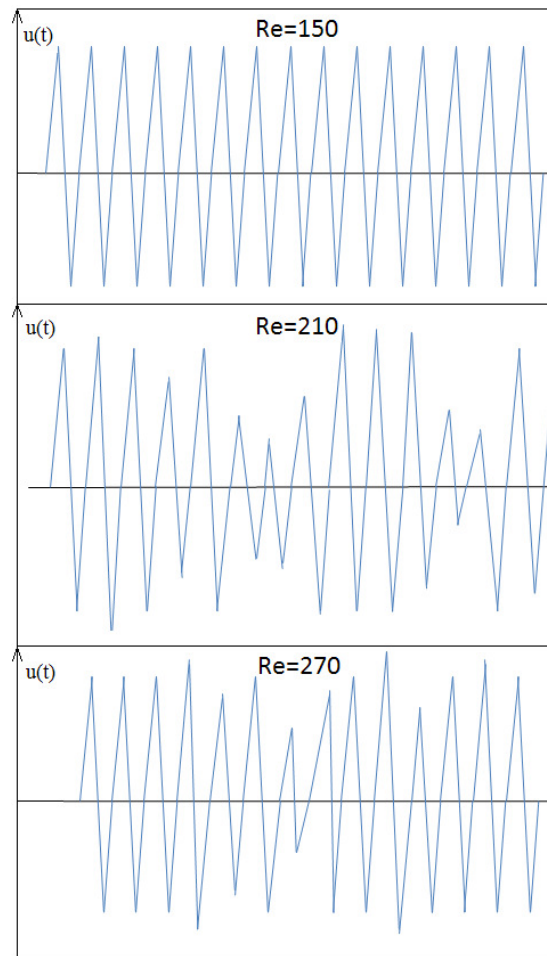


Figure 15*: Velocity oscillation in different regimes

2- Mode B shedding

As we mentioned above, mode B occurs on the smaller physical length scale named “Braid shear layer” by Williamson et al (Williamson, 1996a). As seen in Figure 9 this wavelength in mode B is close to one time the diameter against four times the diameter for mode A. It appears that the instability of mode B is not related to the waviness of the primary vortex as in mode A, because these deformations in mode B are very uniform along their length. The instabilities in mode B are strongly linked to the reverse flow in the near wake but in a different manner than those in mode A. The closeness of the forming braid shear layer to the previously formed braid shear explains the origin of instabilities. On the other hand, the same phenomenon explains why the streamwise vortices are in-phase in mode B. The fact that the new streamwise vortices are formed very close to the previous ones allows them to have the same form. See figure 16.

In other words in-phase streamwise vortices mean that a vortex pair in one braid will be followed by a vortex pair with the same orientation in the next braid. We assume

that the first braid comes from one side of the cylinder and the next braid comes from the other side. See Figures 14 and 16.

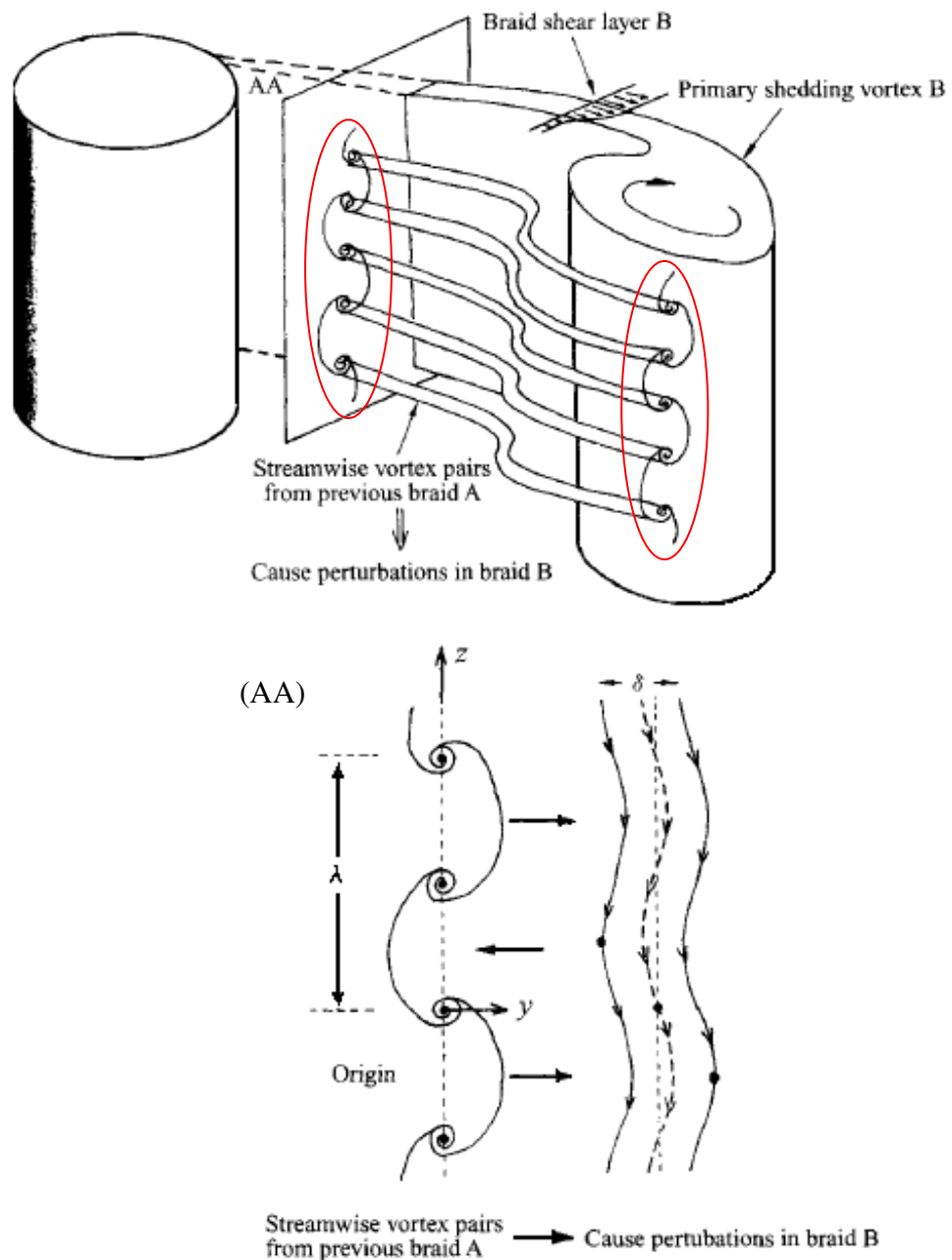


Figure 16*: Physical mechanism in the braid shear layer to produce mode-B streamwise vortices

In figure 16, we show that the presence of the first groups of streamwise vortices (A) close to the forming braid shear layer (B) causes spanwise perturbations on the new shear layer. In perspective view, the line of vortices in braid A will cause spanwise waviness in the new braid shear layer.

3- Characteristics of wake transition

In figure 17 made by Williamson (Williamson, 1996a) we can see the velocity fluctuation in the different shedding regimes: laminar, mode A, mode A-B together and mode B. The first we can see is how turbulent energy decays (loss of energy of vortices) though the wake.

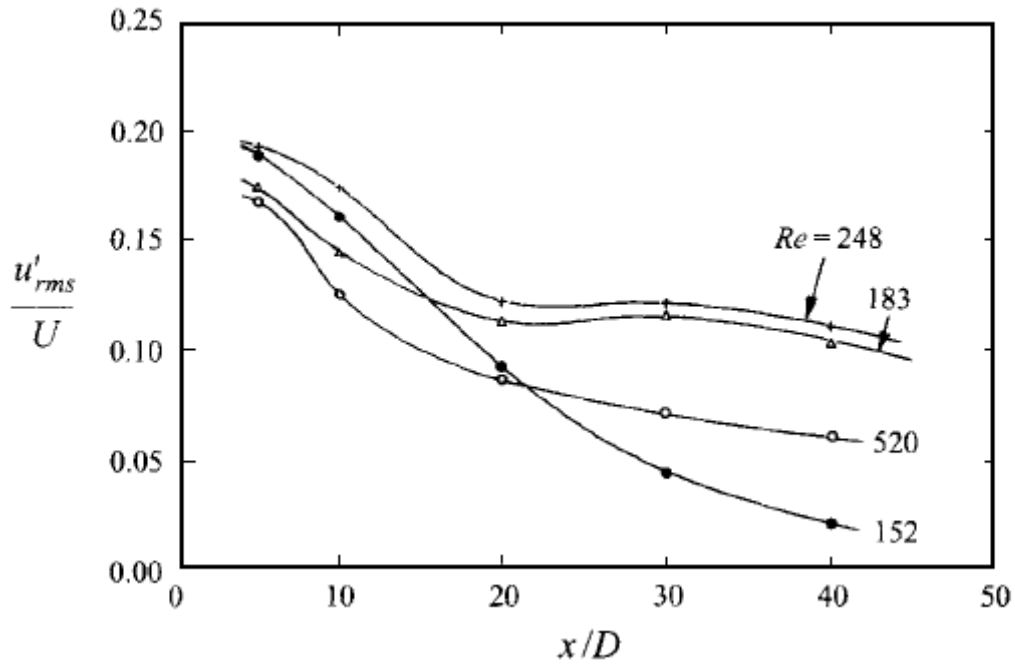


Figure 17*: Turbulent energy decays in the wake, laminar case for $Re=152$, mode A for $Re=183$, mode A and mode B together $Re=248$ and mode B for $Re=520$

The turbulent dissipation (energy dissipation of vortices or vortex strength loss) behind the bluff-body is regular and fast for the laminar regime. While, for the modes A, B and A-B the energy dissipation is slower in the near wake (near wake is around 5 times the diameter). For example in downstream length $40D$, we can observe that for $Re=152$ almost all of turbulence intensity is disappears. However in mode A and mode A-B we just dissipated half of the turbulence energy. We can also point out that in mode A and mode A-B the dissipation rate is lower because of the presence of the low frequency irregularities.

At $Re=260$, we reach a maximum velocity fluctuation and drag coefficient see Figure 6 and 7. The point of $Re=260$ corresponds to the second discontinuity in $S-Re$ curve, and many researchers like Bloor (Bloor, 1964), Prasad & Williamson (Prasad, et al., 1997) suggest that there is possibly resonance frequency at this Reynolds number. This resonance frequency leads the following happening: the changing of shedding mode, the particular ordered streamwise vortex structure in mode B and the end of dislocation phenomenon.

All figures with a star () come from Williamson 1996a, 1996b or Zdravkovich 1997. These figures are also used in order to compare our results shown further in report with them.*

B- THE SIMULATION CODE DESCRIPTION

As reported in introduction the particle deposition and the fluid mechanics phenomena such as vortex shedding are strongly related. In section A the physical phenomenon associated with the fluid mechanics mechanisms has been discussed. In order to have a better understanding of particle deposition we should be able to solve these fluid mechanics problems with a very high accuracy.

Currently, DNS (direct numerical simulation) is one of the few approaches that allow us to have this high precision and to understand the physics of the flow. The simulations with DNS codes have a great similarity with the experiments, as you can see in figure 6 and 13. The goal of this section is to present our simulation code and our initial set up.

I- DNS review

DNS is usually restricted to low Reynolds number, even though this restriction becomes more and more relaxed because of the rapidly increasing power of computers. The number of grid points are related to the Re number as $N \sim Re^{9/4}$. One can ask if DNS is really useful in real life. In fact DNS may not be used for the high Re but it provides us valuable information on the relative magnitudes of the different terms and their scaling in equations. For example, the DNS computations have enabled us to compare the differences between 2-D and 3-D flows at higher Re, in a manner that is not possible in experiment. And it is found that Strouhal number tend to value $S=0.2417$ for large Re. As seen above DNS has shown that this overestimation for Strouhal number (for $Re > 194$) in 2-D case is due to the increase of Reynolds stress.

At the moment, the DNS code is still a research tool, even if this numerical tool is very powerful the normal computers don't have enough capacities to use it. DNS is used for both incompressible and compressible flows; and we can see in our case even with the small inlet velocity and pressure the assumption of compressible flow could be important.

The range of scales that need to be represented in a computation is dictated by the physics. These scales represented by the grid are determinate by numerical method, like different wall law. The Kolmogorov length scale, $\eta = (v^3/\epsilon)^{1/4}$, is usually quoted as the smallest scale that needs to be solved. Here ϵ is the average rate of energy dissipation per unit mass, and ν is the kinematic viscosity of the fluid. However this length scale is very rigorous. The dissipation depends on the energy spectrum and it is greater than Kolmogorov length scale. In Moser and Moin (Moin, et al., 1998) it is indicated that the smallest length scale required in plane channel flows is 12η . It appears that the resolution should be fine enough to capture most of the dissipation statistically.

Spectral methods are used in analytical computation and have a great accuracy. With difference schemes, in order to get the same accuracy we have to use a high order scheme. However, finite difference scheme are typically used in DNS for spatial

resolution because of their lower error level related to the nonlinearity. These nonlinearities error can cause numerical instability or excessive turbulence decay.

Another important factor in DNS is the time advancement. The use of large time steps implies that the small scales can have large errors and this can corrupt the solution. Usually the explicit time step is used in DNS and it is governed by CFL number (*Courant–Friedrichs–Lewy condition*). The timestep must be less than a certain time defines by the equation below.

$$CFL = \frac{u \cdot \Delta t}{\Delta x} \quad (12)$$

When, u is the velocity, Δt the timestep and Δx the length scale. This expression is for one dimension case and it is written just for a view. Basing on sixth order Padé scheme in spatial differencing and fourth order Runge-Kutta scheme in time advancement, Moin (Moin, et al., 1998) showed that the system is unconditionally stable for $CFL < 0.5$, the instability limit is reached for $CFL = 1.43$. In other side the implicit time advancement becomes attractive when the discrete equations represent frequencies far higher than those required by physics. The explicit time advancement is use for convection terms although the implicit one is used for viscous terms.

Specifying boundary conditions at open boundaries is a difficult issue in DNS and the flow compressibility in our case make it harder. Lot of the problems come from acoustic waves in the domain interior, they can influence the inlet flow. These waves could be reflecting by the boundaries, specially the inlet, and corrupt the solution. We had been confronted to same problem in our study. We will argue about this issue in section D.

II- Pencil-code presentation

The goal of this paragraph is to have an overview of the methods which are used in Pencil-code. For more information you can refer to the user manual on internet (Nordita).

The pencil-code is a high order finite-difference code for compressible hydrodynamic flows. We use explicit finite differences, 6th order in space and 3rd order in time. The 6th order in space means that we should have three ghost points at each boundary. The high order schemes are an alternative to spectral or compact schemes, they have the same efficiency and don't need a transpose step. They are also the non conservative scheme that allow us to use a logarithmic density end entropy. The logarithmic schemes increase the convergence of the problem. We can see in Figure 18 the accuracy of different schemes compared with the spectral scheme. The sixth order first and second derivative schemes are given by:

$$f'_i = \frac{-f_{i-3} + 9f_{i-2} - 45f_{i-1} + 45f_{i+1} - 9f_{i+2} + f_{i+3}}{60\delta x} \quad (13)$$

$$f_i'' = \frac{2f_{i-3} - 27f_{i-2} + 270f_{i-1} - 490f_i + 270f_{i+1} - 27f_{i+2} + 2f_{i+3}}{180\delta x^2} \quad (14)$$

When f is a function, f' his first derivative, f'' his second derivative and δx is a grid cell in X direction. High-order centered-difference convection simulations often show “wiggles” (Nyquist zigzag pattern) in $\ln \rho$, which are apparently caused by a velocity profile where the velocity approaches zero on the boundary or inside the box.

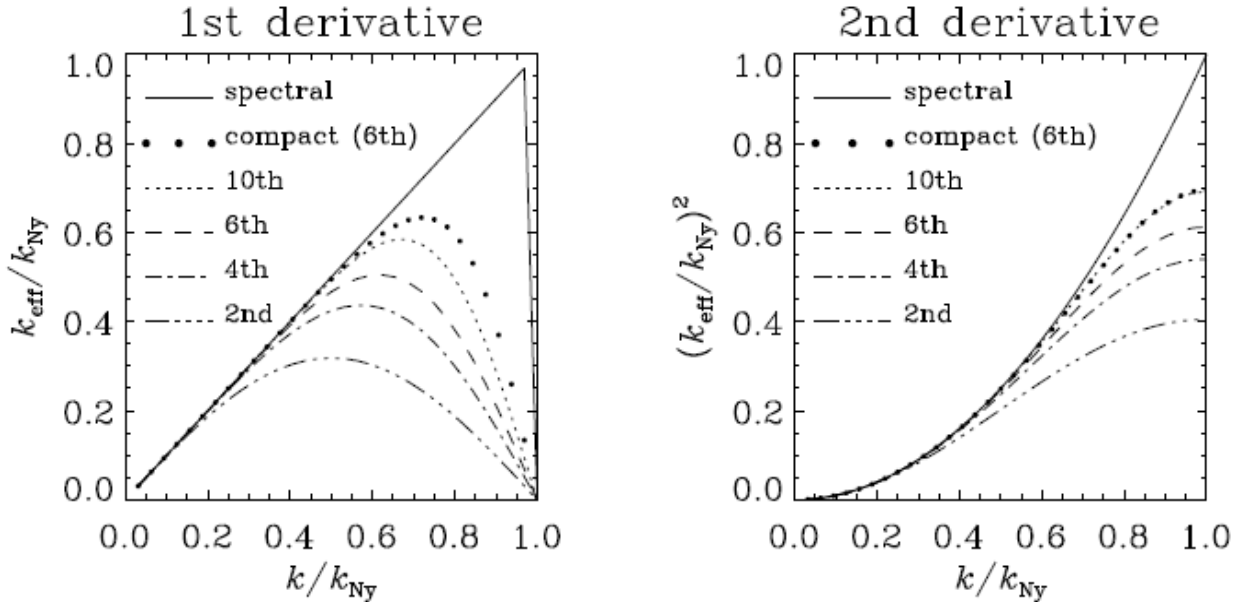


Figure 18: Effective wave numbers for first and second derivatives using different schemes

For time stepping, higher-order schemes are necessary in order to reduce the amplitude and phase errors of the scheme and, to some extent, to allow longer time steps. We use a 2N scheme, for more information on can refer to manual.

The code can also run under Multiprocessing by Message Passing (MPI) on parallel shared or distributed memory computers and the maximum resolution depend on the number of processors than one uses. The pencil-code started in 2001 and currently it is maintained and developed by more than 100 persons. It is highly modular can be easily be adapted to different types of problem. Each run directory has a file (*src/Makefile.local*) in which you choose certain modules like entropy, magnetic fields, hydrodynamics, forcing, etc, which tell the code the variables than it has to resolve. For example if one choose hydrodynamics module, the code would just evaluate the variables concerning this module. The equations solved of the pencil-code are (1) and (2) for the fluid and (3) and (4) for the particles.

Input parameters like boundary conditions or mesh refinement (*which are set in the files 'start.in', 'run.in'*) can be changed without recompilation. Furthermore, one can change the list of variables for monitoring (diagnostic) output on the fly, and there are mechanisms for making the code reload new parameters or exit gracefully at the end of runtime. For using the Pencil-MPI code you can use it on any UNIX system with a F90/F95 compiler. If you have, you will be to be able to visualize the results we use IDL as well, but other tools such as Python or Tecplot can also be used

The mesh refinement and boundary conditions will be discussed in the next sections.

The pencil-code uses a version of immersed boundary method in order to represent solid geometries inside the domain. The current implementation is based on a high order extension of the discrete forcing approach with ghost cells (Mittal, et al., 2005)

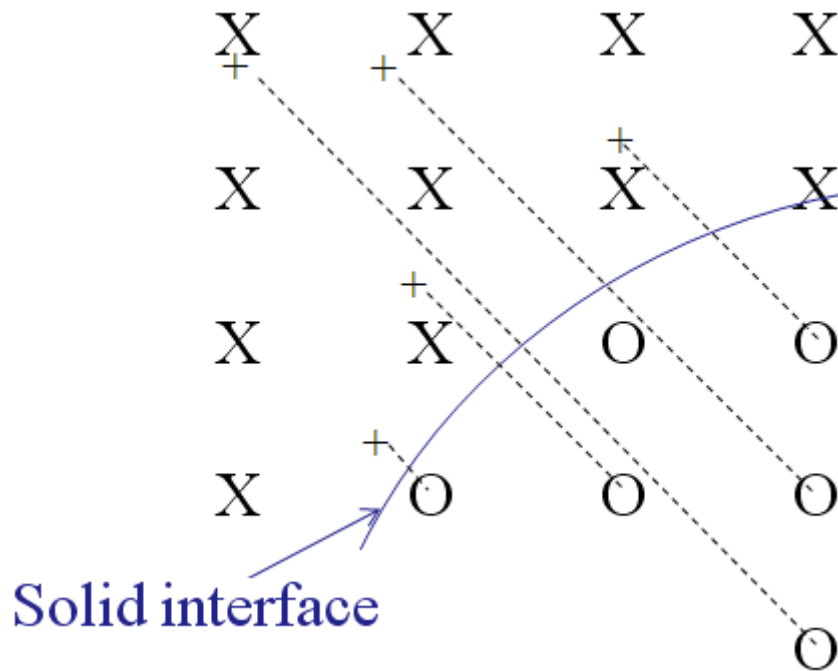


Figure 19: sketch of mirror point's purpose

The pencil-code as we mentioned above is a 6 order central difference code, than 3 point are required in each side of calculated point. This means that if we are in a fluid point very close to the fluid solid interface we will need three points inside the solid geometry. As the points inside the solid are not solved we need some other way of defining their values. This is done by defining a mirror to each point in the solid geometry. In Figure 19 the grid point are symbolized by 'X' and the point inside the solid geometry are symbolized by 'O'. the '+' sign denote the mirror point. The values of mirror point are found by a linear interpolation.

C- RESULTS AND ANALYSIS

I- Simulation approach

At the beginning of our study, we decided to check the validity of our simulation code, the Pencil-code. As reported in sections B and C, the particle deposition is strongly related to the fluid mechanics phenomenon like the vortex shedding. We choose to evaluate the Strouhal number; this number is the fundamental parameter characterizing the instabilities in the wake. Based on works of Williamson (Williamson, 1989; Williamson, 1992), shown in Figure 6, we attempted to reproduce the same curve by our code.

As full three dimensional simulations are very CPU intensive, we have chosen to test the code in two dimensions in order to save computation time. That should give us an important indication on code reliability, for example we will know if our boundary conditions work correctly and which one is more adapted to our cases, ripen the resolution or try the different grid set up. The initial conditions mentioned here have been held constant for all of the simulations: inlet velocity ($u_0=5$ m/s), Cylinder diameter ($D= 33.7 \cdot 10^{-3}$ m) and temperature ($T=600^\circ\text{C}$).

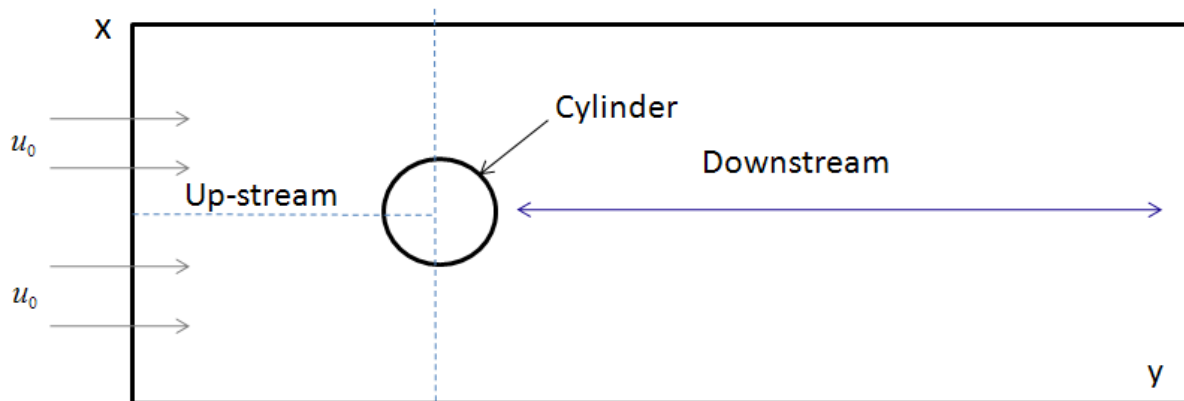


Figure 20: Two dimensional sketch of our box

The first simulations are carried out in a small domain of 0.2 m by 0.4 m and $Re=84$. The boundary conditions are periodic in x , constant inlet velocity for $Y1$ (bottom boundary in y direction), non-reflecting inlet on $Y2$ (top boundary in y direction), the resolution is set equal to 128×256 and cylinder position is invariable. The Strouhal number found was $S=0.188$, which was significantly different from the expected value $S = 0.157$. In order to find the correct result we decided to focus on the following points:

- Resolution and grid set up
- Dimensions of domain
- Boundary conditions set up

The results of these tests are provided in table 1.

1- Dimensions and resolution

Quickly we understood that rising only the resolution had no significant influence on the Strouhal number without a modification of the domain size or boundary conditions.

This is why we have focused on domain size and resolution. As can be seen in table 1, we started to increase the downstream length (in y direction) with a constant resolution, nevertheless the results remained incorrect. We then decided to increase

the width, the downstream length, resolution and, finally, the upstream length in the box.

We found two central features which affected strongly the Strouhal number value: the width of the box and the upstream length.

We have found the correct value of the Strouhal number corresponding to $Re = 84$ for a domain of 2.4 m by 2.4 m with a resolution of 1536x1536 grid points. It must be noted that 2.4 is equal to 71 times the diameter of our cylinder, in other words $x = y = 2.4 \text{ m} = 71D$.

x	y	Resolution	S
0.2	0.4	128x256	0.1881
0.2	0.4	256x512	0.1880
0.2	0.8	128x512	0.1850
0.6	0.8	384x512	0.1685
1.2	0.8	384x512	0.1648
1.2	0.8	768x512	0.1647
1.2	0.8	1536x512	0.1637
2.4	0.8	768x512	0.1672
2.4	1.6	768x1024	0.1620
2.4	2.4	1536x1536	0.1573

Table 1: Strouhal number value function dimension and resolution of domain

Comparing our results with some other works in literature (Wissink, et al., 2008; Luo, et al., 2008) we noted that the size of our domain is larger than what should be required. In those studies mentioned above the width in x direction varies between 10D and 20D, while the length of the box should be around 20D to 25D and the downstream length is equivalent to 15D.

By visualizing the density and velocity profile in our different simulations, especially the ones with the small domains, we find that the inlet boundary in the y direction is affected by some acoustic waves. These waves are not damped at inlet and are reflected back into our domain. This problem is resolved for the outlet by setting some non reflecting boundary, but this kind of boundary condition could not be set up very easily at inlet. The fact that we require almost a constant velocity and density at the inlet complicate the implantation of a non reflecting boundary at the inlet. After these observations we decided to test some new boundary conditions.

2- Boundary conditions

Concerning the boundary conditions in the pencil-code, there are many different types. The choice of them depends on the environment of the problem. In 2-D or 3-D cases the boundary conditions in the z direction are periodic, in the first case we assume that the cylinder is infinite and in the second case it permits us to avoid the

wall influences and the problems related to the end conditions. Some of the different boundary conditions implanted in the Pencil-Code, and use for our simulations, are:

- ‘p’ periodic boundary condition
- ‘a’ asymmetric condition w. r. t. the boundary, i. e. vanishing value
- ‘s’ symmetric condition w. r. t. the boundary, i. e. vanishing first derivative
- ‘a2’ antisymmetry w. r. t. the arbitrary value on the boundary, i. e. vanishing second Derivative
- ‘c1’ special boundary condition for $\ln p$ and s : constant heat flux through the boundary
- ‘set’ set boundary value
- ‘e2’ extrapolation

Different boundary conditions can be set for each element in different directions For example $\text{bcX} = \text{'s'}, \text{'s'}, \text{'s'}, \text{'s'}$ mean that each element corresponds to one of the variables, which are those of the variables like, u_x , u_y , u_z and $\ln p$...

We believe that in the last case listed in table 1, which give a correct Strouhal number, the large size of our box avoids the effects of acoustics waves. But such a large domain (2.4 m and 1536 cells in each direction) would require a lot of time in 3-D simulations. Referring to J.G. Wissink, W. Rodi (Wissink, et al., 2008) we choose a free-slip condition along the walls which means:

- The velocity normal to free slip wall should be zero ($u_x = \text{'a'}$)
- The gradient of the velocity parallel to wall should be zero; the wall shear stress is zero for free slip case. ($u_y = \text{'s'}$)

We use a non reflecting boundary for the outlet flow in Y2 and we specify the velocities conditions at the inlet, $\mathbf{u} = (0.0, 5.0, 0.0)$. These new boundary conditions allow us to divide the domain dimensions by 2 in x direction and 3 in y direction.

3- Grid set up

The set up of a non-equidistant grid should help us to reduce the number of grid cells as the requirements on the resolution is highest close to the cylinder and in the cylinder wake. The grid points must be much denser in the middle of the domain than near the walls. The two following grid functions allow us to realize this meshing approach.

We introduce a non-equidistant grid as a function $= z(\zeta)$ of an equidistant grid ζ_i with grid spacing $\Delta\zeta = 1$. The way the parameters are handled, the box size and position are not changed when you switch to a non-equidistant grid, i.e. they are still

determined by z_0 and L_z (bottom and upper positions of the box for concerned direction). For a general monotonic function $\psi ()$

$$z(\zeta) = z_0 + L_z \frac{\psi[a(\zeta - \zeta_*)] + \psi[a(\zeta_* - \zeta_1)]}{\psi[a(\zeta_2 - \zeta_*)] + \psi[a(\zeta_* - \zeta_1)]} \quad (15)$$

Where Z_0 and Z_0+L_z are the lowest and uppermost levels, ζ_1 , and ζ_2 are the ζ values representing those levels (normally $\zeta_1 = 0$, $\zeta_2 = N - 1$ for a grid of N point), and ζ_* is the ζ value of the inflection point of the $\psi ()$ function. For more information you are referred to the Pencil-Code manual (nordita).

The first grid function is 'Sinh' (hyperbolic sinus function i.e. 'sinh' = $\psi ()$) which allow us to have 'almost' an equidistant grid in the middle. The size of cells near the walls or in the middle can be changed by the coefficients defined in the general function. For example for 'sinh' we should define the inflection point which defines the position of smallest cell and we can also use a 'grid-coefficient' in order to define the difference of the cells size between the smallest and the largest. See figure 21.

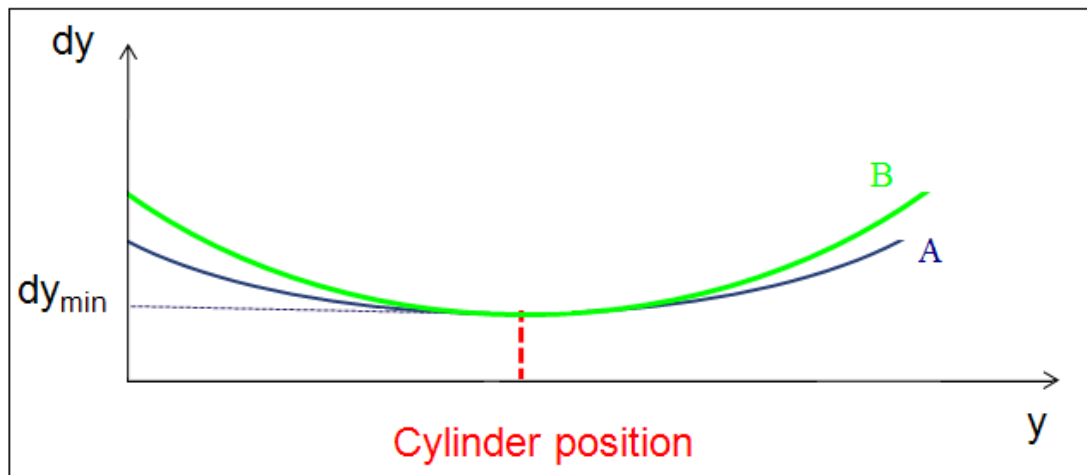


Figure 21: View of cell size for the 'sinh' function with the same inflection point but using different 'grid-coefficient'

However, some simulations didn't get the adequate results when this function was used to set up the mesh. The problem comes from the fact that sometimes we need very small cells behind the cylinder over a great length. To overcome this problem we chose 'step-linear' instead the 'sinh' function. The 'step-linear' function helps us to have an equidistant grid over a certain distance, see Figure 22. The correct results have been found with this new function. We also have the possibility to include other functions if required.

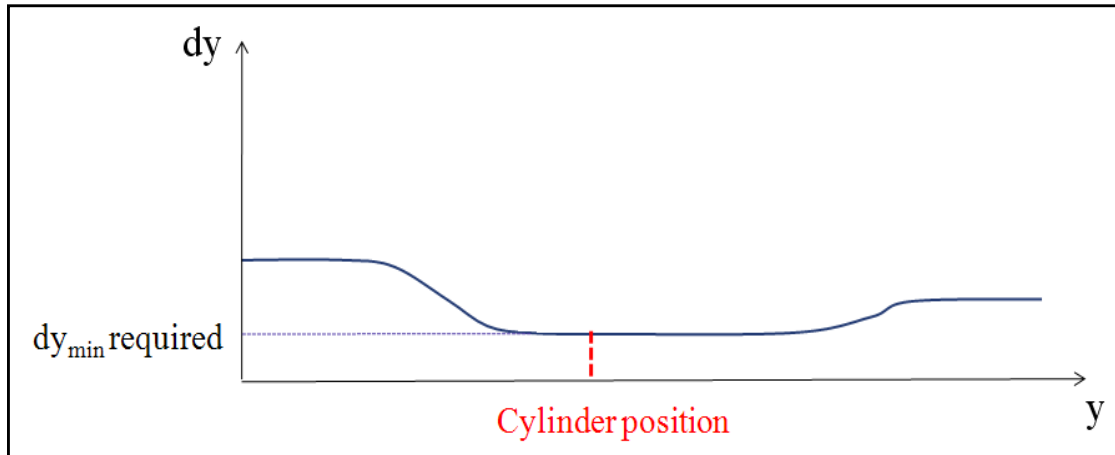


Figure 22: mesh refinement according to step-linear functions

However we have tried to insert a buffer zone, in order to obtain good Strouhal numbers with the same domain sizes as the other works present in literature (Williamson, 1988; Williamson, 1989)

4- Buffer zone

The aim of the buffer zone is to damp all waves arriving at the boundary from inside the domain, and in this way create a non reflecting boundary. The buffer zone is a part of the domain near a boundary, when the fluid is in this area we add an additional term to the Navier-Stokes equation which allow us to reach the values fixed by the user, i.e. the waves are damped (Colonius, et al., 2002). In others term, if $f ()$ represent the N-S equation and $df ()$ is the first derivative of this function we have the following operations:

$$f()_{i+1} = f()_i + df().dt \quad (16) \text{ Normal equation}$$

$$f()_{i+1} = f()_i + \alpha .df().dt \quad (17) \text{ Equation in buffer zone}$$

At the beginning we set up this buffer zone in x and y directions. In y direction for the inlet boundary in order to damp the pressure waves. Since the width of the box (seen in table 1) also has an important role in yielding the correct Strouhal and Reynolds number relation we use the buffer zone in the x direction as well. The simulations show wiggles in the buffer zones, especially at the inlet (see Figure 23). However, since the wiggles never exist outside the buffer zone itself, it seems clear that they will not affect the main simulation. The new domain is 25D in y direction 14D in x direction. In z direction the length should be between 8D or 10D according to the work of (Wissink, et al., 2008; Luo, et al., 2008)

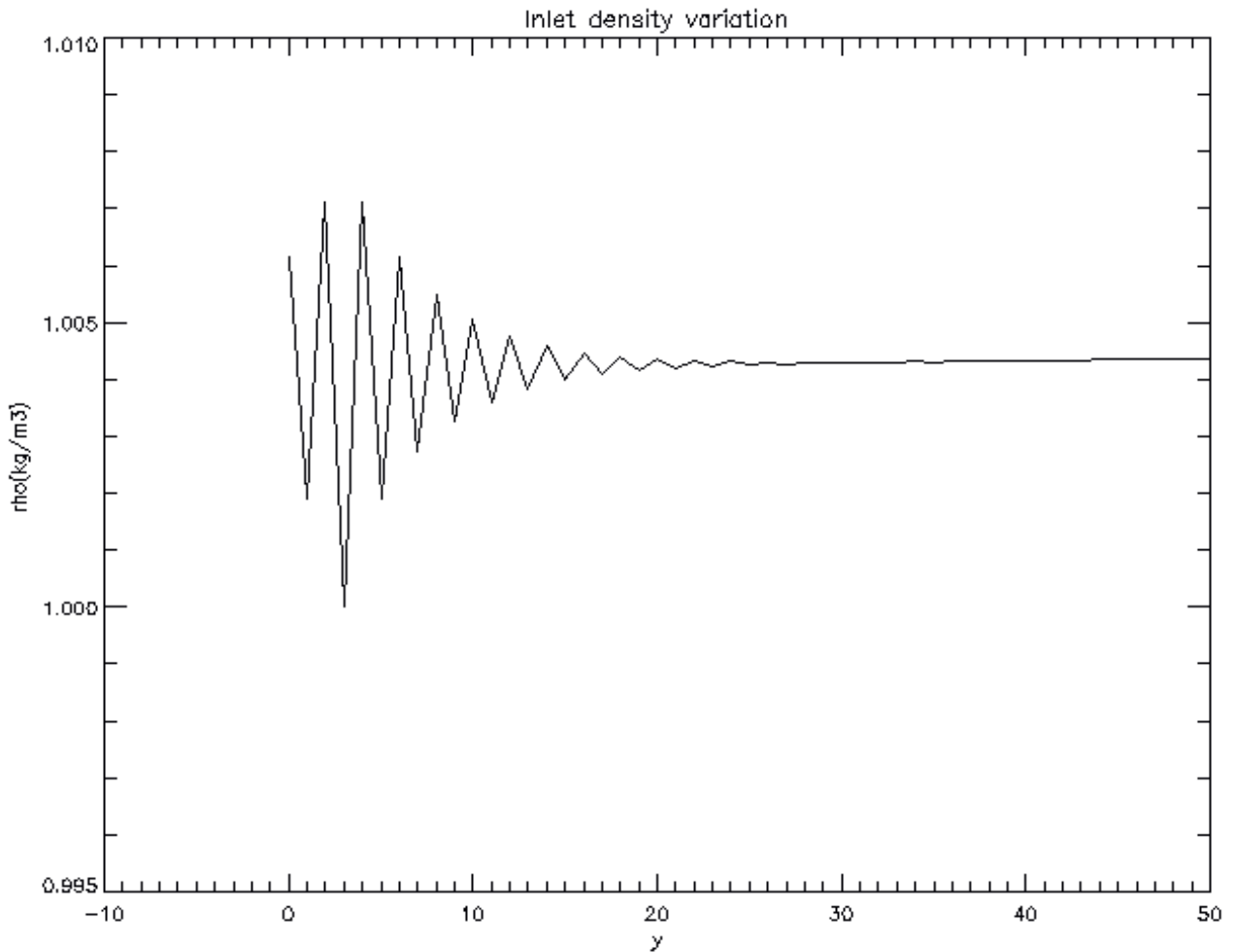


Figure 23: Wiggles in the density at the inlet

The results of all of the modification and different simulations are presented in the next section.

II- Results

In this section we present different results for some 2-D and 3-D cases.

1- Results for 2-D simulation

As seen in section B.II.3 for $Re < 47$, the wake comprises a steady recirculation region (L_w) of two symmetrically placed vortices on each side of the wake. The length of the wake grows as the Reynolds number increases. This phenomenon has been measured experimentally many times, and the pink curve in Figure 24 shows the theoretical evolution of this phenomenon. We tried to reproduce the same curve with the pencil-code (gray curve). In order to evaluate the reliability of our code, the same curve has been measured with another code based on Reynolds Averaged Navier–Stokes (RANS) (blue curve and red points).

As you can see there is an excellent accordance between DNS and RANS calculations. However, these curves are not very close to the theoretical curve but they

are very close with the Taneda (Taneda, 1956) works, who measured this recirculation length for a very long cylinder (2000D) i.e. without any end or wall influence.

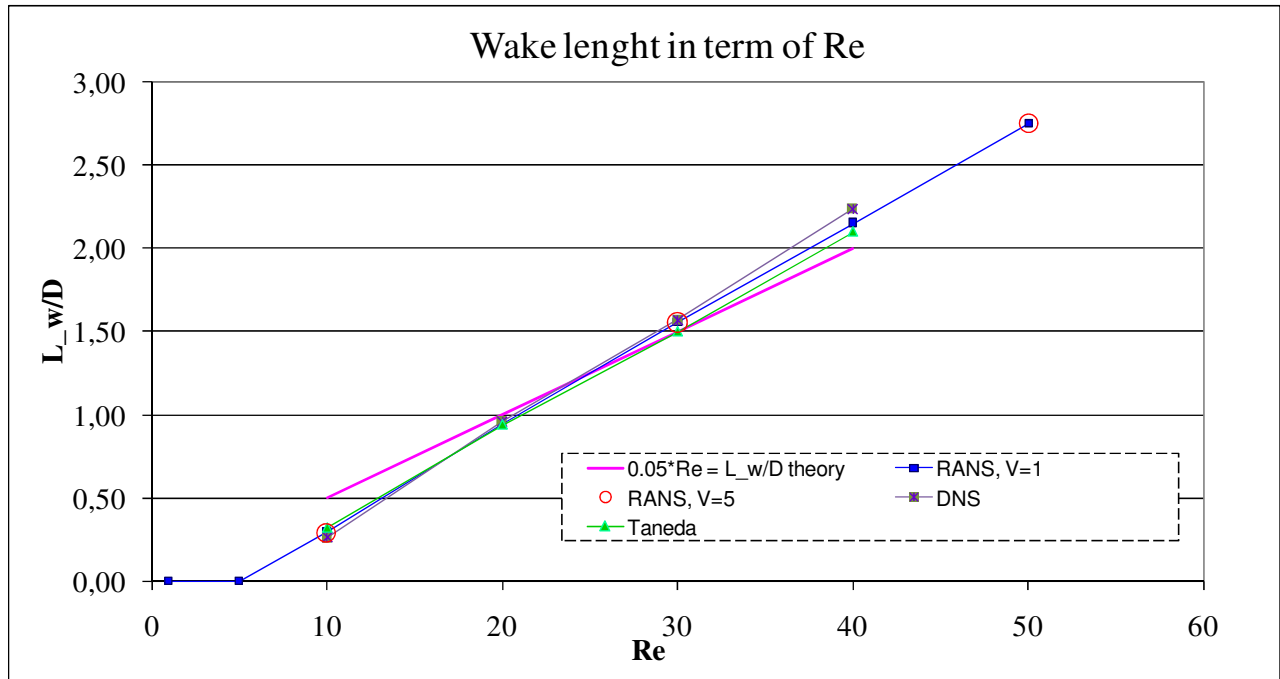


Figure 24: Wake length in term of Re number

The boundary conditions are periodic in the x direction, none reflecting at the outlet and reflecting at the inlet. The resolution is 768x768 (non-equidistant grid) for a box with 2.4 m in each direction. Once these results were confirmed, we focused on unsteady flows, i.e. with $Re > 47$, and the occurrence of eddies in the wake.

In figure 25 the green curve represents the Williamson (Williamson, 1996a) works (experimental works for $40 < Re < 190$ and simulations works for $190 < Re < 400$) in two dimensions and they are usually used as a reference in literature. The other curves correspond to our simulations with pencil-code and their different boundaries conditions.

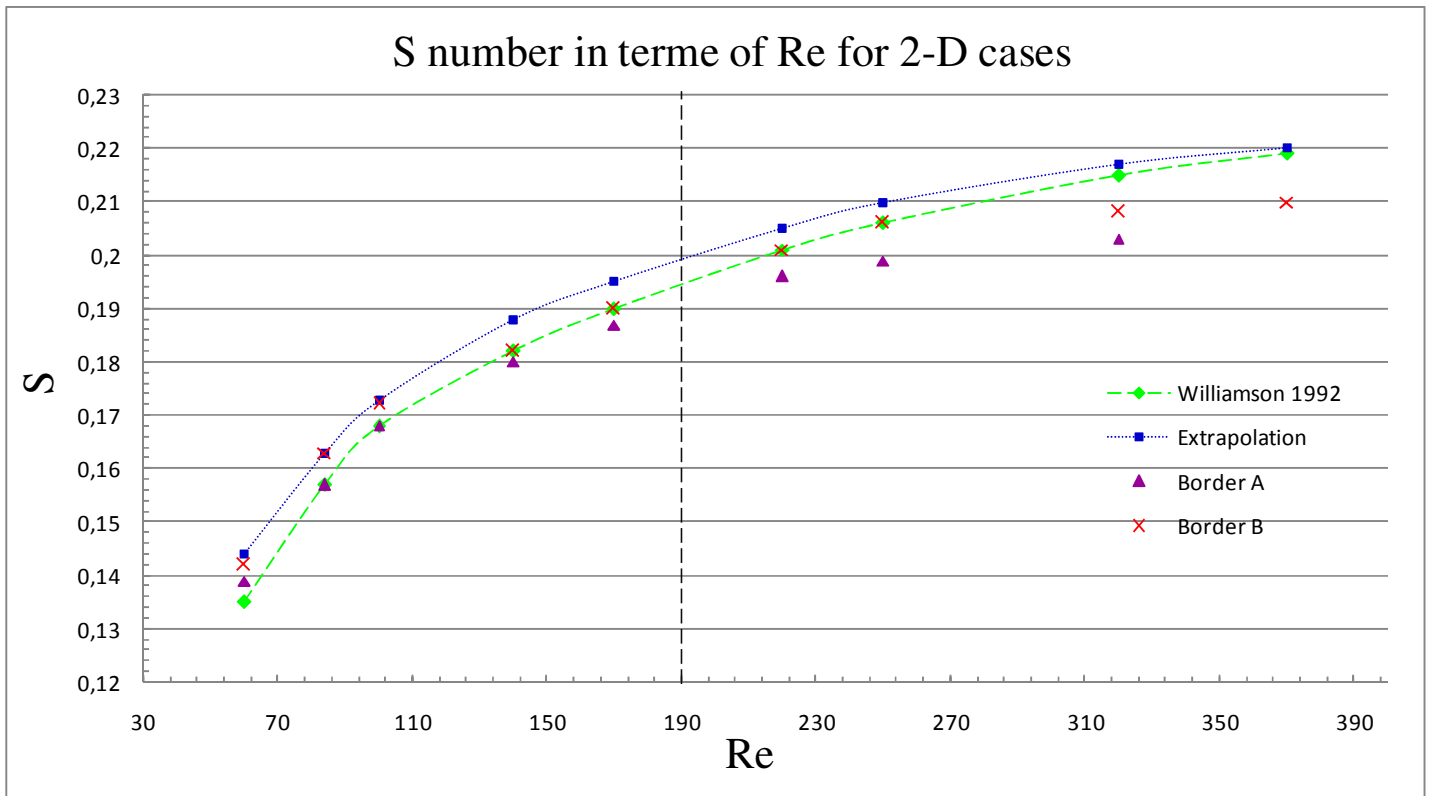


Figure 25: Strouhal number evolution with Re number. Green curve present shows the Williamson works. The blue curve represents the periodic boundary condition in lateral direction. The pink and purple points correspond to free-slip boundary conditions in lateral direction and using of buffer zone at inlet, for the pink curve the length of the buffer zone is 30% smaller while the target on velocity is set for purple curve.

In the present study, the extent of the computational domain in the lateral (x) and the streamwise (y) directions have been set to be 14D and 25D according to paragraph D.I.1. For all of the simulations non-slip boundary conditions are applied to the surface of the circular cylinder. At the inlet boundary, a uniform inlet velocity profile is set as $U = (0, 5, 0)$ and the density is set equal to one. At the outlet boundary, a non-reflective boundary condition is used.

The blue curve shown in figure 25 represents the periodic boundary condition in lateral direction, when the pink and purple correspond to free-slip boundary conditions in lateral direction, using of buffer zone at inlet. As you can see there are two different curves with the buffer zone, they are actually related to the buffer zone conditions like length of the zone or the target on velocity or density. For purple curve the length of the buffer zone is 30% larger and we set a target for the velocity at inlet. For the pink curve we use just the buffer zone condition with a length equal to 1.6D. These two curves indicate that more Re decrease more the acoustics wave (pressure wave) affect the boundary conditions value and the buffer zone conditions should become stronger, this is also one on the main reason why we can't set an unchanged buffer zone. However we have some wiggles at inlet in y direction but they remain in this artificial zone (buffer zone).

We decide to use for the moment boundary conditions for the blue curve, i.e. periodic condition in x direction without any buffer zone. We can point out that the more the Reynolds number is increased, the more that precision is improved. This means that

the boundary conditions are less and less affected by the acoustic waves. This supposition can be very useful for our simulations in 3-D, because in 3-D cases, if we are able to reproduce the shape of the real curve (figure 6), we can either neglect or accept the inaccuracy of the S-Re relation.

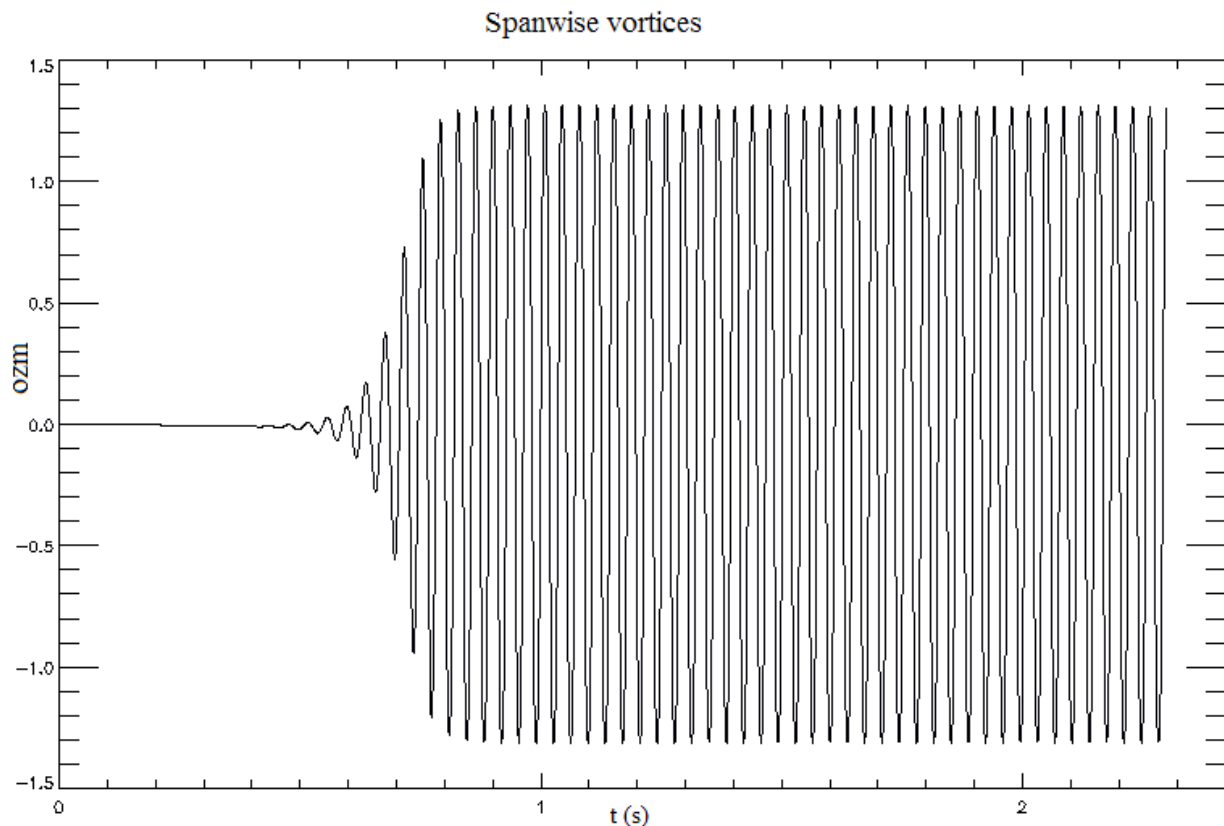


Figure 26: appearance of vortex shedding

Figure 26 shows the vorticity in the z direction as a function of time. We find the frequency of our vortex shedding process by counting the number of peaks for t bigger than 1s.

2- 3-D simulations

Since it is the first time we use pencil-code with the solid geometry implantation in three dimensional cases, we chose to check the code for a high Re number and small box in order to be sure it works properly. For $Re = 500$ we can see the occurrence of streamwise vorticity after 0.8s. We set periodic boundary conditions in the z direction and the extent of the computational domain has been set to be 8D. We want to find the deep part and the discontinuities in S-Re relation, as seen in curve figure 6.

On the other hand we have done some simulations for Re around 700 to have a view about the precision of our code for the vortex shedding in mode B too. The figures 27 and 28 show the switch of 2-D vortex shedding over the mode B of 3-D vortex shedding for Re equal 710. In figure 27 we point out that the velocity fluctuation (here ozm) becomes unpredictable and scattered as mentioned above in section B.III. In figure 28 we visualize the development of streamwise and spanwise vorticity in the same moment. The Strouhal number is equal 0.211 which is very close to the results that one can find in literature (Williamson, 1996a; Williamson, 1996b).

2D and 3D vortex shedding over the time

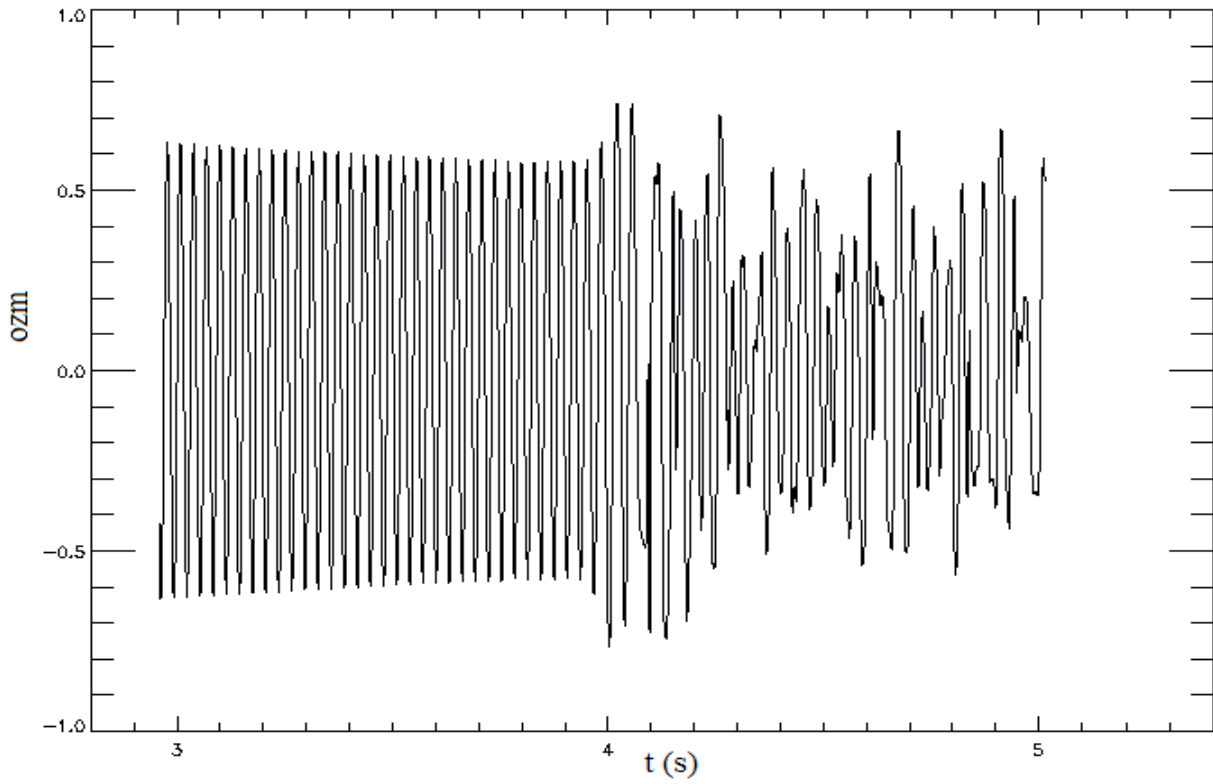


Figure 27: Switch of shedding mode form 2-D to mode B of 3-D

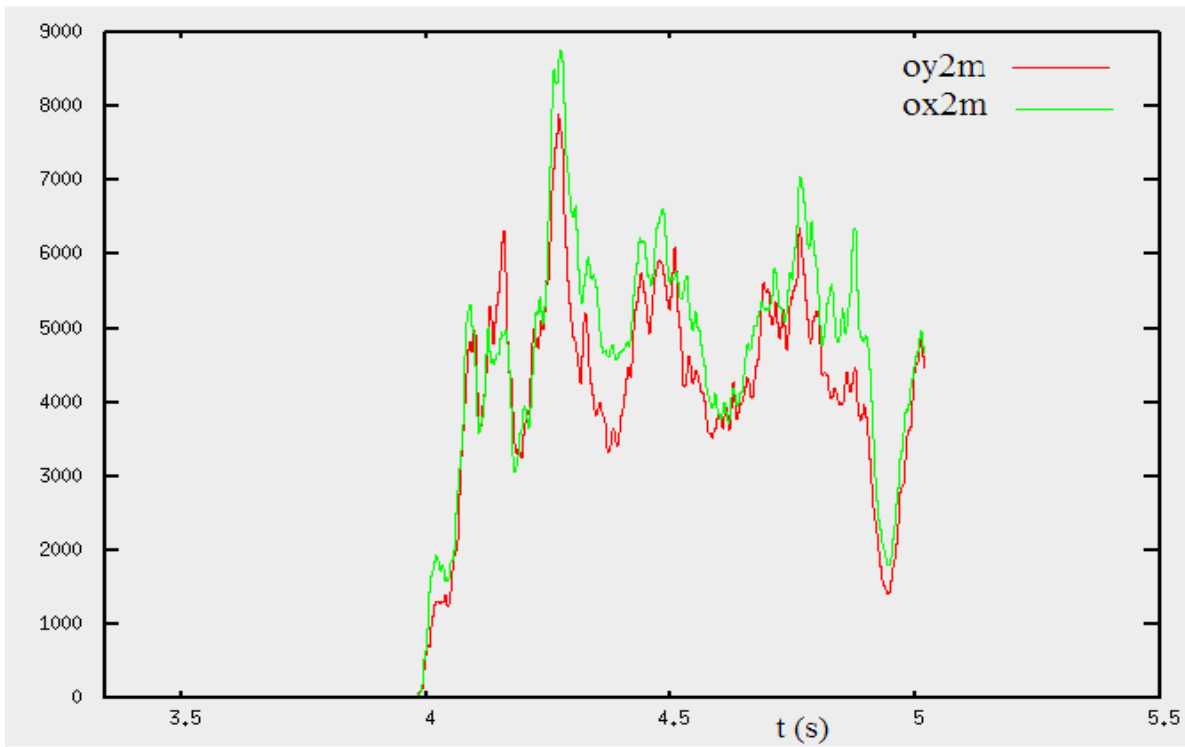


Figure 28: Occurrence of streamwise in x and y directions

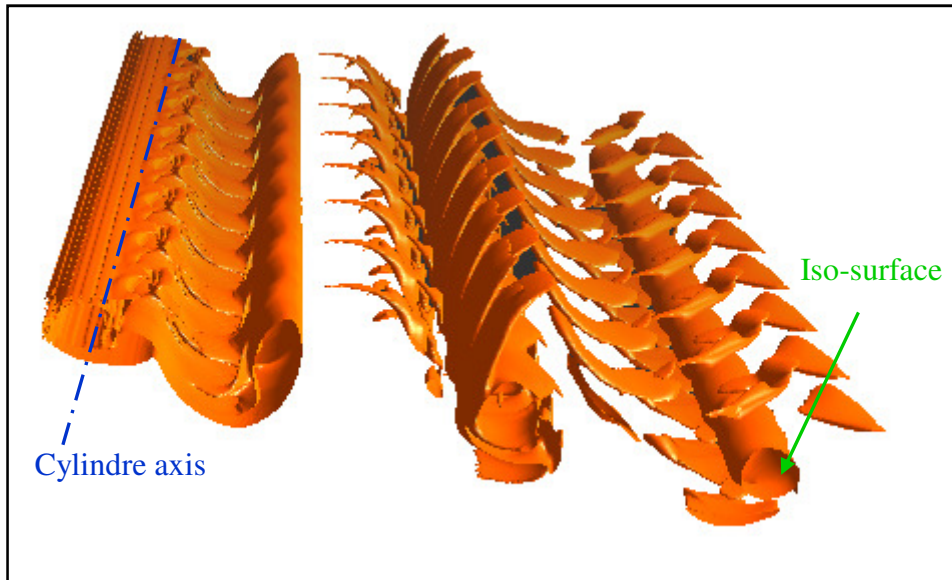


Figure 29: Overview of iso-surfaces and streamwise in the wake for $Re=710$

In figure 29, we can see the view of iso-surface (spanwise) and the streamwise along the cylinder wake. As expected, the increasing Re number lessened the impacts of acoustics wave at the inlet boundary. However we were not able to get the mode A of vortex shedding in 3-Dimensional wake. For $Re=220$ we don't have any streamwise vorticity, and we think that this point is related to the boundary conditions, because the mode A of the vortex shedding is due to elliptical instabilities unlike mode B which is governed by a hyperbolic instability.

III- Critical view

As we could see in the different figures and tables, the results found by the pencil-code when using a large or a small computational domain have a really good accordance with the other studies.

For the small box, 2 dimensional cases give results that are very close to the other experimental and theoretical works, where the error is less than 10%. Sometime by adding some additional terms to our equations we are even able to reduce the error further, see the curves in figure 25. The simulations in three dimensional wakes for $Re > 500$ give a really good agreement with the reality, with a Strouhal number close to 0.21.

However, as has been pointed out throughout the report, there are some points that should be improved, particularly the boundary conditions at the inlet and the set up of the non-reflecting condition. The computation time can be very long in some cases and a high-quality mesh points set up has a central role on this aspect, standing to reason that the number of processors used for the simulation is also an important factor.

Inserting turbulence at the inlet should help us obtain even more realistic simulations in the future, as the real world is seldom perfectly laminar.

Conclusions

The physical and theoretical sides of 2-D and 3-D vortex shedding have been exposed, in particular waketransition regime. As reported, the 2-D shedding mode goes up to a Reynolds number of approximately 190 and it could take place in two different manners, parallel or oblique, which depends strongly to the end and wall conditions along the cylinder.

The switch of 2-D shedding toward 3-D is associated with two discontinuous changes in the wake formation as Re is increased, see Figure 6. The wake transition state of flow is associated with transition to turbulence in the wake. This means that all eddies are formed as laminar and become turbulent downstream. $Re=190$ first discontinuity takes place at $Re = 190$ and it is named “hard transition” in opposition with the second one, which is also hysteretic. In the second discontinuous change in the $St-Re$ relation, there is a gradual transfer of energy from mode A shedding to a mode B shedding over the range 240-250.

The aim of the study was to define all of these dynamic processes in order to have a better view on particle deposition phenomenon, as mentioned above these two different processes are strongly related. The different simulations show that pencil-code could be very useful; results that have been found have a really good agreement with other studies in literature. In 2 dimensional cases we have a really good agreement with the other experimental and theoretical works, with error less than 10%. Sometimes, by setting some additional terms to our equations, we are also able to reach the exact solutions (see the curves in figure 25). The simulations in three dimensional wakes for $Re > 500$ give a really good agreement with reality, the Strouhal number is close to 0.21, and the error is less than 2%.

Even if all of objectives could not be achieved during this internship, we defined areas for future study on this subject. The grid function and the computational domain dimension have been defined with a good accordance with other DNS studies. Consequently, the next step of the study could be the some boundary conditions set up for the non reflecting boundary. Once this is done, the set up of the particles deposition subroutine should not be a problem in three dimensional simulations. Furthermore, the particle deposition study could also be carried out thanks to the turbulence implantation at inlet boundary.

Appendix

Appendix A: Hopf bifurcation

Before any explication on Hopf bifurcation, there are some mathematics terms to know.

Limit cycles: In mathematics or in dynamical systems, a limit-cycle on a plane or a two-dimensional manifold is a closed trajectory in phase space having the property that at least one other trajectory spirals into it either as time approaches infinity or as time approaches minus-infinity. Such behavior is exhibited in some nonlinear systems. In the case where all the neighboring trajectories approach the limit-cycle as time $t \rightarrow \infty$, it is called a stable or attractive limit-cycle. Stable limit-cycles imply self sustained oscillations.

The laminar steady regime is associated with a recirculation region, named wake length. When one increases the Reynolds number, there is a critical Re over which appears wake instability, and it is associated with a sudden growth in amplitude of wake fluctuation and the establishment of periodic laminar wake. This regime transfer is a manifestation of Hopf bifurcation. The idea is that the oscillations in the near wake and the instabilities in the wake are related. "In physical terms, the instability characteristics of a flow are determined by the behavior of its impulse response" (Williamson, 1996a), the system is at the limit of the stability, if a small perturbation is generated the system would have an exponential response and becomes unstable.

The Hopf bifurcation corresponds to the destabilization of a fixed point in order to create a limit cycle. Oscillations of finite amplitude appear suddenly in point of bifurcation, and stay continually in steady state. The amplitude of the cycle is zero at the point of bifurcation.

Bifurcation theory is the mathematical study of changes in the qualitative or topological structure of a given family. A bifurcation occurs when a small smooth change made to the parameter values (the bifurcation parameters) of a system causes a sudden 'qualitative' or topological change in its behavior. Bifurcations occur in both continuous systems (described by differential equations), and discrete systems.

The normal form of a Hopf bifurcation is:

$$\frac{dz}{dt} = z(\lambda + b|z|^2),$$

Where z , b are both complex and λ is a parameter. Write $b = \alpha + i\beta$.

The number α is called the first Lyapunov coefficient. $z(t) = re^{i\omega t}$

By using figure 30 we try to link this equation with the fluid dynamics and in particular with our case. The blue curves correspond to the stable solution, and the

dotted line to unstable. Behind certain point, critical point, the system had two different solutions for the same value. And if the system passes over this critical point, it starts to oscillate continually in steady state and create a limit cycle.

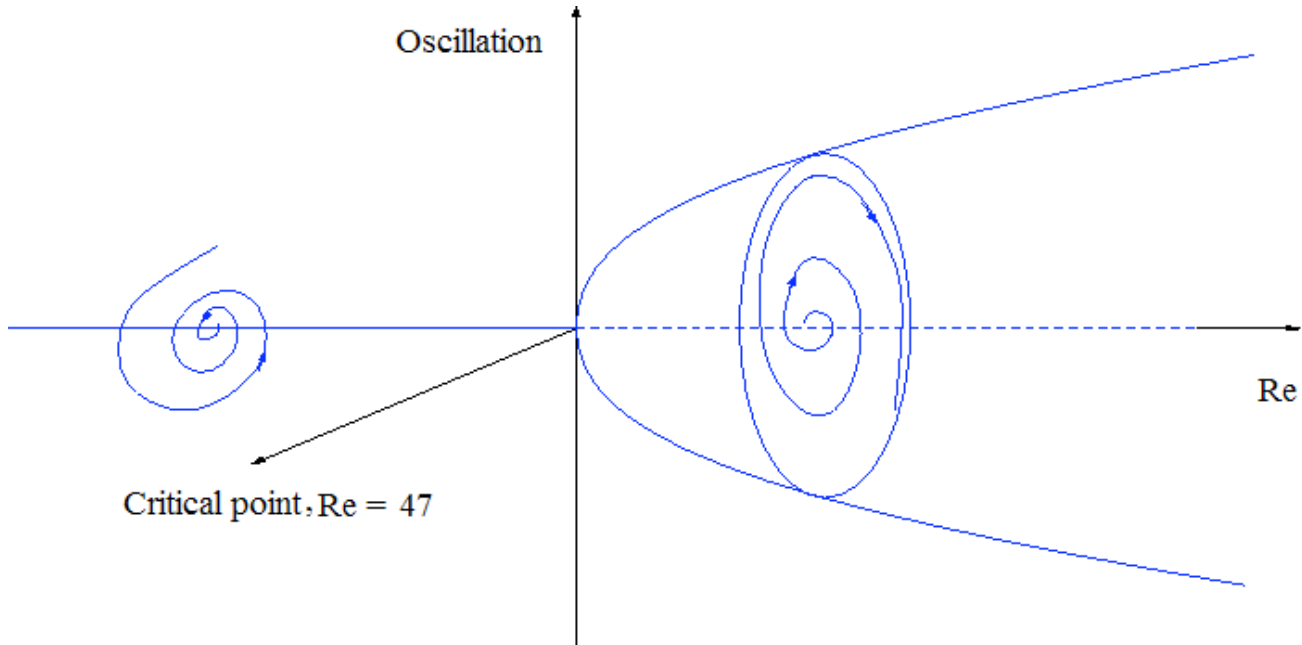


Figure 30: View of Hopf bifurcation

Bibliography

- Bloor MS** The transition to turbulence in the wake of a circular cylinder [Journal] // J. Fluid Mech. - 1964. - pp. 19-290.
- Burger M et al** DNS of droplet–vortex interaction with a Karman vortex street [Journal] // International journal of heat and fluid flow. - 2006. - pp. vol. 27, no2, pp. 181-191.
- Colonus Tim and Ran Hongyu** A Super-Grid-Scale Model for Simulating Compressible Flow on Unbounded Domains [Journal] // J. of computational Physics. - 2002. - pp. 191-212.
- Eisenlohr H and Eckelmann H** Vortex splitting and its consequences in the vortex street wake of cylinders at low Reynolds number [Journal] // Phys. Fluids A. - 1989. - pp. 1-189.
- Gerrard JH** The mechanics of the vortex formation region of vortices behind bluff bodies [Journal] // J. Fluid Mech. - 1966. - pp. 25-401.
- Kamiadakis GE and Triantafyllou GS** Three dimensional dynamics and transition to turbulence in the wake of bluff objects [Journal] // J. Fluid Mech. - 1992. - p. 238.
- Leweke T and Williamson CHK** Three-dimensional instabilities in wake transition [Journal] // European Journal of Mechanic. - July-August 1998. - pp. 571-586.
- Luo K and Fan J** Transient, three-dimensional simulation of particle dispersion in flows around a circular cylinder $Re = 140-260$ [Journal] // Fuel. - 2008. - 88. - pp. 1294- 1301.
- Miller GD and Williamson CHK** Control of three-dimensional phase dynamics in a cylinder wake [Journal] // Exp. Fluids. - 1994. - pp. 18-26.
- Mittal R and Balachandar S** Effect of three dimensionality on the lift and drag of nominally two-dimensional cylinders [Journal] // Phys. Fluids. - 1995. - pp. 71-184.
- Mittal R and Iaccarino G** Immersed Boundary Methods [Journal]. - [s.l.] : Annual Review of Fluid Mechanics, 2005. - Vol. 37. - pp. 239-261.
- Moin P and Mahesh K** Direct Numerical Simulation: A Tool in turbulence Research [Journal] // Annu. Rev. Fluid Mech. - 1998. - pp. 539–78.
- Monkewitz PA, Williamson CHK and Miller GD** Three-dimensional phase dynamics in a wake [Journal] // Bull American Physical Society. - 1993. - pp. 38-2303.
- Nordita** Pencil-code [Online]. - 11 08 2009. - <http://www.nordita.org/software/pencil-code>.
- Prasad A and Williamson CHK** Three-dimensional effects on turbulent bluff body wakes at moderate Reynolds numbers [Journal] // J. Fluid Mech. - 1997. - pp. 564-602.
- Roshko A and Fiszdon W** On the persistence of transition in the near wake. In Problems of Hydrodynamics and Continuum Mechanics [Journal] // Philadelphia: SOCI.n d. Appl. Math. - 1969. - pp. 606-16.
- Roshko A** Experiments on the flow past a circular cylinder at very high Reynolds number [Journal] // J. Fluid Mech. - 1961. - pp. 10-345.
- Sobey IJ** Oscillatory flows at intermediate Strouhal number in asymmetry channels [Journal] // Journal of Fluid Mechanics. - 1982. - pp. 359-373.
- Taneda S** Expreimental investigations of the wake behind cylinders and plates at low Reynolds numbers [Journal] // Journal Physical Society Japan. - 1956. - pp. 302-7.
- Waleffe F** On the three-dimensional instability of strained vortices [Journal] // Phys. Fluids. - 1990. - pp. 2-76.

- Wikipedia** Hopf bifurcation overview [Online]. - 08 11, 2009. - http://en.wikipedia.org/wiki/Hopf_bifurcation.
- Williamson CHK** Oblique and parallel modes of vortex shedding in the wake of a circular cylinder at low Reynolds numbers [Journal] // J. Fluid Mech. - 1989. - pp. 206-579.
- Williamson CHK** The existence of two stages in the transition to three dimensionality of a cylinder wake [Journal] // Phys. Fluids. - 1988. - pp. 31-3165.
- Williamson CHK** The natural and forced formation of spot-like dislocations in the transition of a wake [Journal] // J. Fluids Mech. - 1992. - pp. 243-393.
- Williamson CHK** Three-dimensional wake transition [Journal] // J. Fluids Mech. - 1996b. - pp. 345-407.
- Williamson CHK** Vortex dynamics in the cylinder wake [Journal] // Anna Rev Fluid Mech. - 1996a. - pp. 477-539.
- Wissink JG and Rodi W** Numerical study of the near wake of a circular cylinder [Journal] // Int Journal Heat Fluid Flow. - 2008. - pp. 1060-70.
- Zdravkovich MM** Flow around circular cylinders, Volume 1: Fundamentals [Book]. - [s.l.] : Oxford Science Publications, 1997. - 0198563965.